NASA TECHNICAL NOTE

NASA TN D-3871

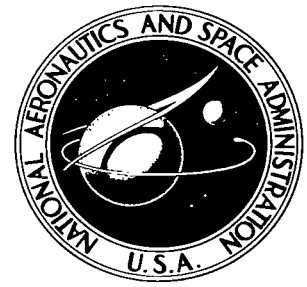

NASA TN D-3871

EFFECT OF ROUGHNESS ON HEAT TRANSFER TO HEMISPHERE CYLINDERS AT MACH NUMBERS 10.4 AND 11.4

by James C. Dunavant and Howard W. Stone

Langley Research Center
Langley Station, Hampton, Va.

NATIONAL AERONAUTICS AND SPACE ADMINISTRATION • WASHINGTON, D. C. • MARCH 1967

EFFECT OF ROUGHNESS ON HEAT TRANSFER TO HEMISPHERE CYLINDERS AT MACH NUMBERS 10.4 AND 11.4

By James C. Dunavant and Howard W. Stone

Langley Research Center
Langley Station, Hampton, Va.

NATIONAL AERONAUTICS AND SPACE ADMINISTRATION

For sale by the Clearinghouse for Federal Scientific and Technical Information
Springfield, Virginia 22151 – CFSTI price $3.00

EFFECT OF ROUGHNESS ON HEAT TRANSFER TO HEMISPHERE CYLINDERS AT MACH NUMBERS 10.4 AND 11.4

By James C. Dunavant and Howard W. Stone
Langley Research Center

SUMMARY

Heat-transfer and pressure distributions on hemisphere-cylinder models have been presented at nominal Mach numbers of 10 and 11 over a free-stream Reynolds number range of 0.77×10^6/m to 7.4×10^6/m (0.23×10^6/ft to 2.2×10^6/ft). The 0.15-m (6.0-in.) diameter models had round-protuberance roughened surfaces with heights of 0.63 mm and 1.26 mm (0.025 in. and 0.050 in.), a random nodular roughened surface with an average height of 0.1 mm (0.004 in.), and a reference smooth surface. The results indicate the roughness elements did not increase the heat transfer at the stagnation point, on the hemisphere, or on the cylinder when the flow remained laminar. At the higher Reynolds numbers, heating rates characteristic of transitional boundary layers were measured on the hemispherical part of several roughened models. On the cylindrical part of the model downstream of the transitional flow, heat rates equal to those of the smooth model were observed. The calculated momentum thickness Reynolds numbers at transition were very low, between 25 and 55.

INTRODUCTION

Reentry and high-speed cruise vehicles may have rough aerodynamic surfaces for several reasons; among these are manufacturing techniques, expansion joints, buckling and local distortion due to heating, and – in the case of ablating bodies – ablation-induced roughness as shown in references 1 to 3. If the surface roughness promotes transition from laminar to turbulent flow, an increase in aerodynamic heating occurs. Some investigators have found that even if transition does not occur, certain types of roughness may increase laminar boundary-layer heating. These factors have prompted a number of studies of the interplay of roughness and heating.

Exploratory tests of models at supersonic speeds have shown that uniformly distributed roughness may increase heating. On smooth and rough hemisphere-cone models, Diaconis, et al. (ref. 4) found that a sand-blast roughness increased laminar heating over the hemisphere and part of the cone by 50 percent at $M = 3.12$. Strass and Tyner (ref. 5) found similar increases in the heat transfer to flat disks with various machine groove

surface roughnesses at M = 2. Nikuradse (ref. 6) in a classical experiment of the effect of roughness using a pipe found that roughness did not change the skin friction as long as the flow was laminar. In studying the effect of several two-dimensional distortion elements at hypersonic speeds, Bertram and Wiggs (ref. 7) found very high peak heating and slightly higher average heating to a two-dimensional model with a single sine wave in the surface; Rhudy and Magnan (ref. 8) found little change in the average heating rate to a flat plate with a series of sine-wave surface distortions.

To extend the experimental knowledge to axisymmetric bodies with three-dimensional roughness in hypersonic flows, the present study employed hemisphere-cylinder models with roughened surfaces and smooth surfaces; these models were tested at Mach numbers of 10.4 and 11.4. The investigation was undertaken to determine the effect of roughness on stagnation heating, the heating distribution around the body, and the parameters that correlated the heat transfer to the rough surfaces. The pressure and heat-transfer distributions to four rough models and a smooth model were measured over a free-stream Reynolds number range of 0.77×10^6/m to 7.4×10^6/m (0.23×10^6/ft to 2.2×10^6/ft).

SYMBOLS

c_w	specific heat of wall material
D	model diameter
h	heat-transfer coefficient
K_w	thermal conductivity of air at wall
k	roughness height (see fig. 6)
l	spacing between successive rows of roughness (see fig. 6)
M	Mach number
N_{St}	Stanton number based on free-stream conditions
p	pressure
R_D	free-stream Reynolds number based on model diameter

s	surface distance from stagnation point
T	temperature
t	wall thickness
u	velocity
z	spacing between roughness elements (see fig. 6)
γ	ratio of specific heats
δ^*	boundary-layer displacement thickness
θ	boundary-layer momentum thickness
μ	viscosity
ρ	density
τ	time
ϕ	meridian angle defined in figure 6
ψ	angle from stagnation point on hemisphere

Subscripts:

aw	adiabatic wall conditions
e	local conditions at edge of boundary layer
sm	reference condition, stagnation point of smooth model
t	total
w	wall
o	stagnation point

∞	free-stream conditions
2	conditions behind normal shock

APPARATUS AND METHODS

Tunnel and Injection Strut

The tests were conducted in the nominal Mach 10 and 11 nozzles of the Langley continuous-flow hypersonic tunnel. A general view of the tunnel is shown in figure 1. Each nozzle is water cooled and has a 78.7-cm (31-in.) square test section. The test gas, air, was preheated in electrical resistance tube heaters to 1200° K (1700° F) for the Mach 11.4 tests, and 978° K (1300° F) for the Mach 10.4 tests. Stagnation pressures used in the tests were from 2.42×10^6 N/m^2 (350 psi) to 8.27×10^6 N/m^2 (1200 psi) at $M_\infty = 11.4$ and 2.42×10^6 N/m^2 (350 psi) to 10.4×10^6 N/m^2 (1800 psi) at $M_\infty = 10.4$.

Figure 2 is a schematic diagram of the facility. The Mach 10.4 tests were conducted with the facility operating continuously; that is, the tunnel was in the closed loop system with the compressors. The Mach 11.4 tests, however, were conducted in an extended blowdown operational mode in which high-pressure air is taken from the storage bottles, expanded through the tunnel, and returned to atmospheric pressure through the compressors.

The Mach 11.4 nozzle with a water-cooled stainless-steel throat was calibrated from pressure measurements near the stagnation point of the hemisphere-cylinder models. The pressure measurements at the $\psi = 10^{\circ}$ station were corrected to stagnation point ($\psi = 0$) values by modified Newtonian theory to obtain the calibration shown in figure 3(a).

A water-cooled beryllium-copper throat was used for the Mach 10.4 tests. The calibration of the Mach 10.4 nozzle shown in figure 3(b) was made with a total-pressure probe at or near the tunnel center line for the lower pressure part of the calibration. The high-pressure part of the calibration was obtained in the same manner as the Mach 11.4 calibration. The instrument accuracy for the pressure measurements results in a Mach number uncertainty which is within the brackets or the symbol itself shown in the figure.

Prior to testing, the models are positioned in an injection chamber mounted on the side of the tunnel (fig. 4) where they are cooled to room temperature. One of the hemisphere-cylinder models is shown mounted on the injection strut in the retracted position in figure 5 (chamber removed from tunnel). The high-pressure air cooling tubes can be seen on the four sides of the chamber. The model was rapidly injected into the

hypersonic airstream and the pressure and temperature data were recorded automatically on magnetic tape by an analog-to-digital converter at intervals of 0.05 second.

Models

Four hemisphere-cylinder models were constructed from 0.8-mm (1/32-in.) inconel sheet for this test program. The surfaces of three of the models were roughened by pressing rounded protuberances into the surfaces by means of male and female dies. The protuberances were arranged in rows normal to the flow direction and, where possible, the protuberances in successive rows were behind the gap in the row ahead. The height and spacing of these protuberances are shown in the table in figure 6 (models II, III, and IV).

The fourth model was a smooth lightly polished model (model I) with a surface roughness, according to interferometer measurement, of 1×10^{-4} mm (4 microinches). After completing the tests of the smooth model, the surface was coated with a molten copper spray; the spraying resulted in a randomly spaced and shaped nodular surface roughness. This model is designated model V. Microscopic examination of model sections after testing showed that a copper coating approximately 0.2 mm (0.008 in.) thick had been evenly distributed over the surface and the average nodule height was 0.1 mm (0.004 in.). Photographs of the five model surfaces are shown in figure 7.

The hemisphere-cylinder models were mounted on the model support system as shown in figure 8. In the assembled configuration, the transducers, shown mounted on the support system, were inside the hemisphere-cylinder which was attached at the trailing edge to the circular plate. The orifice-to-transducer tubing and the thermocouple leads were coupled behind the circular plate and a cylindrical shield was attached to the rear of the model to protect these leads. (See fig. 5.) This close coupling of orifices and transducers resulted in model pressures reaching equilibrium within 2 seconds after injection.

Limited space for transducers on the support system permitted use of only eight orifices per test. The unused orifices on the model were sealed prior to testing. The relative locations of the orifices and thermocouples are shown in figure 6. On the protuberance-roughened models, the orifices were always located in the valleys between the protuberances by displacing (when necessary) the orifice slightly on the periphery. The thermocouples were randomly located with respect to the protuberances since the temperature rise rate at a thermocouple will not depend on its location (top or bottom) on any one protuberance. Initial unequal rates of temperature rise at stations in close proximity are equalized by quickly established temperature gradients and conduction patterns so that regardless of thermocouple location on a protuberance, the rate of temperature rise will represent an average value of heating to the whole protuberance. The surface temperature measurements were monitored to delay the data-reduction period until after

the initial transient temperature rise was completed. This initial transient temperature rise is seen as a change in the slope of a curve for the temperature variation with time and was not observed in these tests to be any greater for the roughened models than for the smooth model.

The wall thickness of the three round-protuberance-roughened models was measured prior to roughening of the surfaces. In the forming process the surface may be thinned or thickened locally on any protuberance but no material is removed. Thus the thickness of the model obtained before roughening is the weight of material per unit smooth model area. To account for the material added on the copper-sprayed model, an equivalent thickness of inconel was added to the thickness of the smooth model. This equivalent amount was determined from the thickness of the copper coating, the relative densities, and the specific heats of inconel and the sprayed copper.

Methods

Pressure instrumentation.- The manufacturers stated accuracies for the three transducers on the orifices nearest the stagnation point are ±1 percent of full scale. The first two transducers were 34×10^3 N/m^2 (5 psi) and the third transducer was 21×10^3 N/m^2 (3 psi) full scale. The remaining transducers were 7×10^3 N/m^2 (1 psi) full scale with a stated accuracy of ±1/4 percent. These lower pressure instruments, however, show a zero shift between calibrations before and after tests of models I to IV and resulted in estimated accuracies of ±50 percent for the lowest pressure measured (0.07×10^3 N/m^2 (0.01 psi)).

Heat transfer.- The heat transfer was obtained by the transient calorimeter technique for which the heat-transfer rate is assumed to equal the rate of heat stored in the surface; thus

$$\dot{q} = h\left(T_{aw} - T_w\right) = \rho_w t c_w \frac{dT_w}{d\tau}$$

For these tests radiation from the surface was negligible. The rate of heat stored was determined by fitting a second-degree polynomial by the method of least squares to a 1-second interval of the recorded temperature data and taking the derivative at the center of the interval. The mass per unit smooth surface area $\rho_w t$ was determined from the smooth-model thickness measurement and density.

The adiabatic wall temperature at each thermocouple location was calculated from

$$T_{aw} = T_t\left(\frac{1 + \eta_r \frac{\gamma - 1}{2} M_e^2}{1 - \frac{\gamma - 1}{2} M_e^2}\right)$$

for a temperature recovery factor η_r equal to $\sqrt{0.7}$. The local Mach number was determined from the isentropic expansion of air from the stagnation-point pressure to the local measured pressure. Real gas relationships were used to determine free-stream and stagnation-point quantities.

Estimates of a lateral conduction error in the measured heat-transfer rates were made by using the method of reference 9. At the stagnation point, the conduction correction to the measured heating rate was less than 1 percent. The heat-transfer data are therefore presented without the conduction corrections.

RESULTS AND DISCUSSION

Pressure Distributions

Representative wall pressure distributions for the five models are presented in figure 9. The wall pressures are effectively divided by a measured stagnation pressure; however, since the pressure was not measured at the stagnation point but 10° away from it, it was corrected to the stagnation pressure according to Newtonian theory. The pressure distributions over the three round-protuberance-roughened models as well as the copper nodule model at all Reynolds numbers are approximately the same as on the smooth model.

The pressure indicated by the data fairing was used with an assumption of isentropic expansion from the stagnation pressure to the local pressure in order to calculate the local flow conditions at the boundary-layer edge for theoretical heat-transfer distributions and other boundary-layer parameters. The validity of the assumption of an isentropic expansion was established by Crawford and McCauley in reference 9 by making pitot surveys of the boundary layer.

Stagnation-Point Heating

The measured heating parameter $N_{St}\sqrt{R_D}$ at the stagnation point of models I to V is presented in figure 10 (solid symbols) as a function of roughness Reynolds number. The values for models I to IV are normalized to the smooth model (model I) values of the same parameter at the corresponding Reynolds number. Because the smooth model was not tested at Mach 10.4, the stagnation heating on model V is normalized by a theoretical value for a smooth model calculated by the method of reference 10. The stagnation-point heating ratio is within ±7 percent of unity for all the models and thus there is no apparent effect of these roughnesses on the stagnation-point heat transfer. The open symbols shown in figure 10 and taken from references 4 and 5 indicate an increase in the heating at the stagnation point with roughness Reynolds number. Strass and Tyner's tests at a Mach number of 2.0 (ref. 5) of disks normal to the flow indicated a general increase in

heating at the stagnation point when the various machine-type surface roughness heights were increased. Diaconis, et al. (ref. 4) tested at $M = 3.12$ only one sand-blast-roughened configuration, a hemisphere-cone; that test indicated an increase in laminar heating with Reynolds number over that of a smooth model.

Although apparent inconsistencies between the references and present data are not explained from the available information, several significant roughness parameters can be identified and are presented in table I. The surface area ratio is the ratio of the actual model surface area with the roughness to the surface area of the model of the same size without surface roughness. In the present tests, the surface area was increased over the smooth-model surface area by as much as 19 percent with no increase in the stagnation-point heat transfer over that of the smooth model. Strass and Tyner, however, had surface area increases of 1 to 38 percent and found stagnation-point heat-transfer increases of 4 to 70 percent.

Maximum values of roughness Reynolds number, both free stream and local (local Reynolds number is much lower than free stream at the high Mach numbers) for the present tests and the references considered are presented in table I. As previously indicated in figure 10, the data of Diaconis, et al. indicated a critical value of free-stream roughness Reynolds number, approximately 50, below which the roughness has no effect on the stagnation heat-transfer rate. The heating ratio from Strass and Tyner and the present investigation does not correlate on this basis for Reynolds numbers based on either free-stream or local conditions.

The roughness number is defined as the ratio of roughness height to the thermal boundary-layer thickness. At the stagnation point it can be shown that for a linear temperature variation in the boundary layer, the thermal boundary-layer thickness is K_w/h_o. The data reported by Strass and Tyner indicate a trend of increasing stagnation-point heat transfer with increasing roughness number; this trend is not shown in the present tests in the range of roughness number.

The roughness ratio also shown in table I is obtained from the roughness height and the boundary-layer displacement thickness at the stagnation point. Boundary-layer displacement thicknesses for a smooth model were calculated by using the method of reference 11. On the basis of k/δ^*, the surfaces of the present roughened models are much rougher than those of the disks and hemisphere-cone of references 4 and 5.

Thus, the present test results at Mach 10.4 and 11.4 are contrary to the reference results even though they are within the range of a number of roughness parameters for which increases in heating at the stagnation point at lower Mach numbers have been shown.

TABLE I.- STAGNATION-POINT ROUGHNESS PARAMETERS

Model	Source	Roughness height		Roughness configuration	Model configuration	Mach number	Surface area ratio	Maximum roughness Reynolds number		Roughness number, kh_{sm}/K_w	Roughness ratio (stagnation point), k/δ^*	Heating ratio, h_o/h_{sm}
		mm	in.					$\frac{\rho_\infty u_\infty H}{\mu_\infty}$	$\frac{\rho_2 u_2 H}{\mu_2}$			
2	Reference 5	0.34	0.013	Bidirectional grooves	Disk	2	[a]1.381	[c]2700	[c]1900	[c]21.2	[c]3.3	1.70
5	Reference 5	0.0263	1035×10^{-6}	Rough machine	Disk	2	[b]1.309	[c]90	[c]64	[c]1.24	[c].26	1.25
6	Reference 5	0.00104	41×10^{-6}	Smooth machine	Disk	2	[b]1.0275	[c]9	[c]6.4	[c].046	[c].0104	1.17
10	Reference 5	2.032×10^{-4}	8×10^{-6}	Smooth machine	Disk	2	[b]1.01	[c]2.2	[c]1.6	[c].008	[c].0020	1.04
Hemisphere	Reference 4	0.0034	130×10^{-6}	Sand blast	Hemisphere	3.12	------	168	64	2.53	.50	1.50
I	Present paper	1.0×10^{-4}	4×10^{-6}	Smooth machine	Hemisphere	11.4	[a]1.00	.32	.024	5.84×10^{-4}	.0020	1.0
II	Present paper	0.6	0.025	Hemispherical pods	Hemisphere	11.4	[a]1.19	1778	150	3.77	12.5	1.02
III	Present paper	0.6	0.025	Hemispherical pods	Hemisphere	11.4	[a]1.05	1580	132	3.40	12.5	1.04
IV	Present paper	1.3	0.050	Hemispherical pods	Hemisphere	11.4	[a]1.19	3690	300	7.43	25	1.0
[d]V	Present paper	0.1	0.004	Copper nodules	Hemisphere	10.4	------	748	58.8	.749	2.0	.98

[a]Calculated from direct measurements.

[b]Calculated from measurements taken directly from photomicrographs of duplicate specimens (ref. 5).

[c]Based on root mean square value of roughness.

[d]Copper nodule.

Heat Transfer to Hemisphere and Cylinder

The heat-transfer distributions for the smooth model and the three models with round protuberances tested at $M = 11.4$ are presented in figure 11. The distributions are presented as the ratio of the Stanton number square root of Reynolds number parameter $N_{St}\sqrt{R_D}$ to the value of the same parameter at the stagnation point of the smooth model at the corresponding unit Reynolds number. In figure 12, the heat-transfer distribution along an element of the hemisphere-cylinder is presented for the copper nodule model (model V) tested at $M = 10.4$. (The heat-transfer distribution data from the $M = 10.4$ test showed no variation with meridian angle ϕ, and only the data for $\phi = 0$ are presented in this figure.) Since the smooth model was not tested at this Mach number, the distributions are presented as the Stanton number square root of Reynolds number parameter $N_{St}\sqrt{R_D}$. As can be seen in figure 11(a) for the smooth model, the laminar heat-transfer parameter $N_{St}\sqrt{R_D}$ is well correlated over the range of test Reynolds numbers when referenced to the stagnation-point value. The same correlation holds for the rough models (figs. 11(b) to 11(d)) except on models II, IV, and V in the region of $s/D = 0.2$ to 0.6 at the high Reynolds numbers. This region on models II, IV, and V will be discussed later. In general, the heating on all models, smooth and rough, compared equally with a theoretical distribution of reference 11 if the regions from $s/D = 0.2$ to 0.6 on the hemisphere at the high Reynolds numbers are not considered.

In order to show the effect of roughness on the heating to the hemisphere and cylinder better, a direct comparison of the heating to the smooth and rough models is presented in figures 13 and 14. The heating is normalized by the measured stagnation-point heat-transfer coefficient of the particular model. Over the range of the test conditions, the round protuberances of model III are observed to have no effect on heating to the hemispherical and cylindrical regions of the model (fig. 13). At the junction of the hemisphere and cylinder of model II, the heating is one-third less at all Reynolds numbers. This one-third reduction is observed only on one ray; on other rays no decrease occurred. In figure 14, the normalized heating distributions of model V at $M = 10.4$ are compared with that of model I (smooth model) at $M = 11.4$. The difference in free-stream Mach number between the tests is expected to have negligible effect on the normalized heating distributions. On the cylindrical portion of the model, the higher heating on model V as compared with model I may be attributed to the higher pressure in this region as compared with the pressures on model 1. (See fig. 9.) As Reynolds number increased from approximately 0.81×10^6, the heating ratio to the hemisphere increased significantly, but along the cylinder the heating ratio decreased with increasing Reynolds number. Whereas these trends are clearly defined in the Mach 10.4 tests in which Reynolds numbers up to 1.12×10^6 were attained, they are less discernible in the Mach 11.4 tests of models II and IV and to an even lesser degree on models I and III which had no upstream increase in heating. A similar decrease with increasing Reynolds number in laminar heating

ratio h/h_o has been observed by others in tests where no region of increased heating upstream was recorded. For example, see references 12 (fig. 9(a)) and 13.

The heating distribution to the region from $s/D = 0.2$ to 0.6 which has been excluded from the previous discussions has a shape which is different from the laminar heat-transfer distributions. The differences are found in this region on all the roughened models except for model III, which had the smaller height, round protuberances, and large spacing. These differences which occur only at the higher Reynolds numbers are characteristic of transitional heating over the hemisphere as indicated in figures 13 and 14. The variation in Stanton number with the Reynolds number for various locations on the model (fig. 15) at $s/D = 0.0872$ indicates that the boundary layer is laminar. At $s/D = 0.349$, the data for models I and III show a laminar variation of heating with Reynolds number; however, on models II and IV the heat-transfer data deviate sharply from the laminar boundary-layer variation at the higher Reynolds numbers. At the shoulder ($s/D = 0.786$) and on the cylindrical portion of the model ($s/D = 1.535$), the heat-transfer data parallel the laminar theory and again signify a laminar boundary layer from the hemisphere-cylinder juncture downstream on the model. The theory presented in this figure uses the distribution calculated by the method of reference 11 and the smooth-model stagnation-point heating value for the various Reynolds numbers.

This same pattern can be seen in a similar series of plots for the $M = 10.4$ data shown in figure 16. At $s/D = 0.044$, the data are clearly laminar except for the one point above a Reynolds number of 1×10^6. At larger values of s/D on the hemisphere, the increasing Stanton number with Reynolds number is indicative of a transitional boundary layer. Downstream of the hemisphere cylinder juncture the heating at all Reynolds numbers again appears to be that of a laminar boundary layer. Sternberg in reference 14 reports an experimental and theoretical investigation of a similar phenomenon in which a turbulent boundary layer returned to a laminar boundary layer under the influence of the strong pressure gradient at the juncture of a cone cylinder. Likewise, Launder (ref. 15) showed that in a favorable pressure gradient, a roughness-induced turbulent boundary layer reverted to a boundary layer which exhibited all laminar boundary characteristics. The heat transfer to the cylinder of the present models appears to result from a similar boundary-layer transition reversal.

The local Reynolds numbers based on boundary-layer momentum thickness calculated by the method of Cohen and Reshotko (ref. 16) is presented in figure 17. The locations of transition for the various models indicated by the symbols on the curve were obtained from the heat-transfer distribution plots in figures 11 and 12. It appears that the local momentum thickness Reynolds number at transition was constant at different unit Reynolds numbers and possibly constant for different roughness sizes, but was not the same at the two free-stream Mach numbers. These values of transition Reynolds

number fall well below the correlation line for natural transition on spheres at $M = 2.0$ and 4.15 presented in figure 14 of reference 17.

In an effort to establish a relationship between the present tests and those of others, the ratio of the roughness height to the boundary-layer displacement thickness will be used as a criterion of comparison. By using the method of reference 11, laminar boundary-layer displacement thicknesses for a smooth surface were calculated for the hemisphere-cylinder model and the test Reynolds numbers as well as for the hemisphere-cone model and test Reynolds numbers of reference 4. The boundary-layer displacement thickness nondimensionalized by the model diameter and Reynolds number for the present $M = 10.4$ tests is shown in figure 18.

The range of the ratio of roughness height to boundary-layer displacement thickness for the present tests and some reference tests is shown as a function of the local Mach number in figure 19. On the basis of the parameter being examined, the sand-blast-roughened hemisphere-cone of reference 4 is seen to be relatively smoother than the models of the present investigation and yet produced increases in the laminar heating not found in the present tests at the same local Mach numbers.

Results of investigations of two-dimensional surface distortion on sharp and blunt flat plates (refs. 7 and 8) are also shown in figure 19. These investigations examined primarily the localized effects of the distortion on heating and may illustrate a possible flow mechanism by which roughness may alter the average heating. Bertram and Wiggs (ref. 7) present the results of two-dimensional surface distortions at $M = 6.8$ and $M = 9.6$. The localized heating showed that separation followed by reattachment occurred on the upstream face of protrusions and on the downstream face of the cavities. At the reattachment points the heat transfer was very high, but, in general, the average heating over the distortion appeared to be only slightly greater than the nondistorted-flat-plate heat transfer. Over most of the Reynolds number range of the tests, the boundary layer downstream of the distortion was laminar.

Rhudy and Magnan (ref. 8) present the results of some tests at $M_\infty = 10$ on a flat plate with two-dimensional multi-cycle full sine-wave distortions. These results show pressure and heat-transfer distributions similar to those of reference 7. However, Rhudy and Magnan found that whenever the boundary layer remained laminar over sections of surface distortion, the integrated heat rate to the distortion section was slightly lower than the smooth-flat-plate value. The average heating to the cycles increased (over the laminar value) when transition occurred.

Although the protuberances on the hemisphere-cylinders are three-dimensional, it is conceivable that a flow pattern of separation and reattachment may be occurring locally as was shown for the two-dimensional distortions of references 7 and 8. When the average heating results of these references are considered, it is not altogether unexpected

that the present results showed no effect of roughness on heating. This absence of heating increase is extended to a lower Mach number range and to a larger number of roughness elements by the present investigation.

CONCLUSIONS

Heat-transfer and pressure distributions on hemisphere-cylinder models have been presented at nominal Mach numbers of 10 and 11 over free-stream Reynolds number range of 0.77×10^6/m to 7.4×10^6/m (0.23×10^6/ft to 2.2×10^6/ft). The 0.15-m (6.0-in.) diameter models had round-protuberance-roughened surfaces with heights of 0.63 mm and 1.26 mm (0.025 in. and 0.050 in.), a random nodular roughened surface with an average height of 0.1 mm (0.004 in.), and a reference smooth surface. The results of this investigation indicate the following conclusions:

1. The roughness elements did not increase the heat transfer at the stagnation point on the hemisphere or on the cylinder when the flow remained laminar.

2. At the higher Reynolds numbers, heating rates characteristic of transitional boundary layers were measured on the hemispherical part of several roughened models. On the cylindrical part of the model downstream of the transitional flow, heat rates equal to those of the smooth model were observed. The calculated momentum thickness Reynolds numbers at transition were very low, between 25 and 55.

Langley Research Center,
National Aeronautics and Space Administration,
Langley Station, Hampton, Va., November 1, 1966,
129-01-09-11-23.

REFERENCES

1. Dow, Marvin B.; and Brewer, William D.: Performance of Several Ablation Materials Exposed to Low Convective Heating Rates in an Arc-Jet Stream. NASA TN D-2577, 1965.

2. Chapman, Andrew J.: An Experimental Evaluation of Three Types of Thermal Protection Materials at Moderate Heating Rates and High Total Heat Loads. NASA TN D-1814, 1963.

3. Dow, Marvin B.; Pittman, Claud M.; and Croswell, William F.: Thermal Performance and Radio-Frequency Transmissivity of Several Ablation Materials. NASA TN D-1896, 1964.

4. Diaconis, N. S.; Wisniewski, Richard J.; and Jack, John R.: Heat Transfer and Boundary-Layer Transition on Two Blunt Bodies at Mach Number 3.12. NACA TN 4099, 1957.

5. Strass, H. Kurt; and Tyner, Thomas W.: Some Effects of Roughness on Stagnation-Point Heat Transfer at a Mach Number of 2, a Stagnation Temperature of 3,530° F, and a Reynolds Number of 2.5×10^6 Per Foot. NACA RM L58C10, 1958.

6. Nikuradse, J.: Laws of Flow in Rough Pipes. NACA TM 1292, 1950.

7. Bertram, M. H; and Wiggs, M. Margarette: Effect of Surface Distortions on the Heat Transfer to a Wing at Hypersonic Speeds. Paper No. 62-127, Inst. Aerospace Sci., June 1962.

8. Rhudy, J. P.; and Magnan, J. D.: Investigation of Heat Transfer and Pressure Distributions in Regions of Surface Distortion on a Flat Plate. AEDC-TDR-62-238, U.S. Air Force, Jan. 1963.

9. Crawford, Davis H.; and McCauley, William D.: Investigation of the Laminar Aerodynamic Heat-Transfer Characteristics of a Hemisphere-Cylinder in the Langley 11-Inch Hypersonic Tunnel at a Mach Number of 6.8. NACA Rep. 1323, 1957. (Supersedes NACA TN 3706.)

10. Cohen, Nathaniel B.: Boundary-Layer Similar Solutions and Correlation Equations for Laminar Heat-Transfer Distribution in Equilibrium Air at Velocities up to 41,100 Feet Per Second. NASA TR R-118, 1961.

11. Crawford, Davis H.: Effects of Laminar-Boundary-Layer Displacement on a Hemisphere in Helium Flow. NASA TN D-2193, 1964.

12. Holloway, Paul F.; and Dunavant, James C.: Heat-Transfer and Pressure Distributions at Mach Numbers of 6.0 and 9.6 Over Two Reentry Configurations for the Five-Stage Scout Vehicle. NASA TN D-1790, 1963.

13. Dunavant, James C.; and Everhart, Philip E.: Investigation of the Heat Transfer to the HL-10 Manned Lifting Entry Vehicle at a Mach Number of 8. NASA TM X-998, 1964.

14. Sternberg, Joseph: The Transition From a Turbulent to a Laminar Boundary Layer. Rept. No. 906, Ballistic Res. Labs., Aberdeen Proving Ground, May 1954.

15. Launder, Brian E.: Laminarization of the Turbulent Boundary Layer by Acceleration. Rept. No. 77, Gas Turbine Lab., Massachusetts Inst. Technol., Nov. 1964.

16. Cohen, Clarence B.; and Reshotko, Eli: The Compressible Laminar Boundary Layer With Heat Transfer and Arbitrary Pressure Gradient. NACA Rep. 1294, 1956. (Supersedes NACA TN 3326.)

17. Beckwith, Ivan E.; and Gallagher, James J.: Heat Transfer and Recovery Temperatures on a Sphere With Laminar, Transitional, and Turbulent Boundary Layers at Mach Numbers of 2.00 and 4.15. NACA TN 4125, 1957.

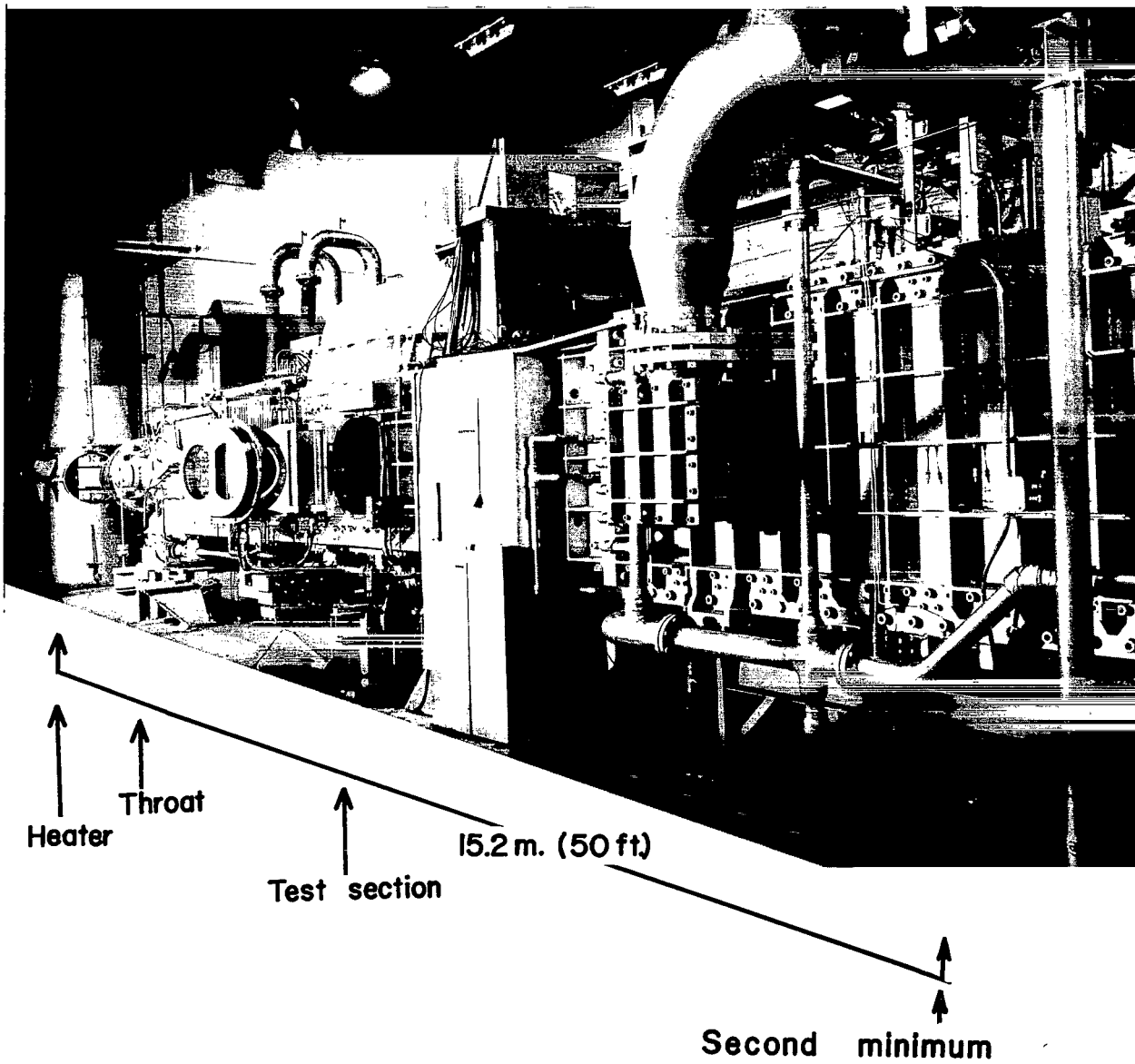

Figure 1.- Langley continuous-flow hypersonic tunnel. L-65-5822

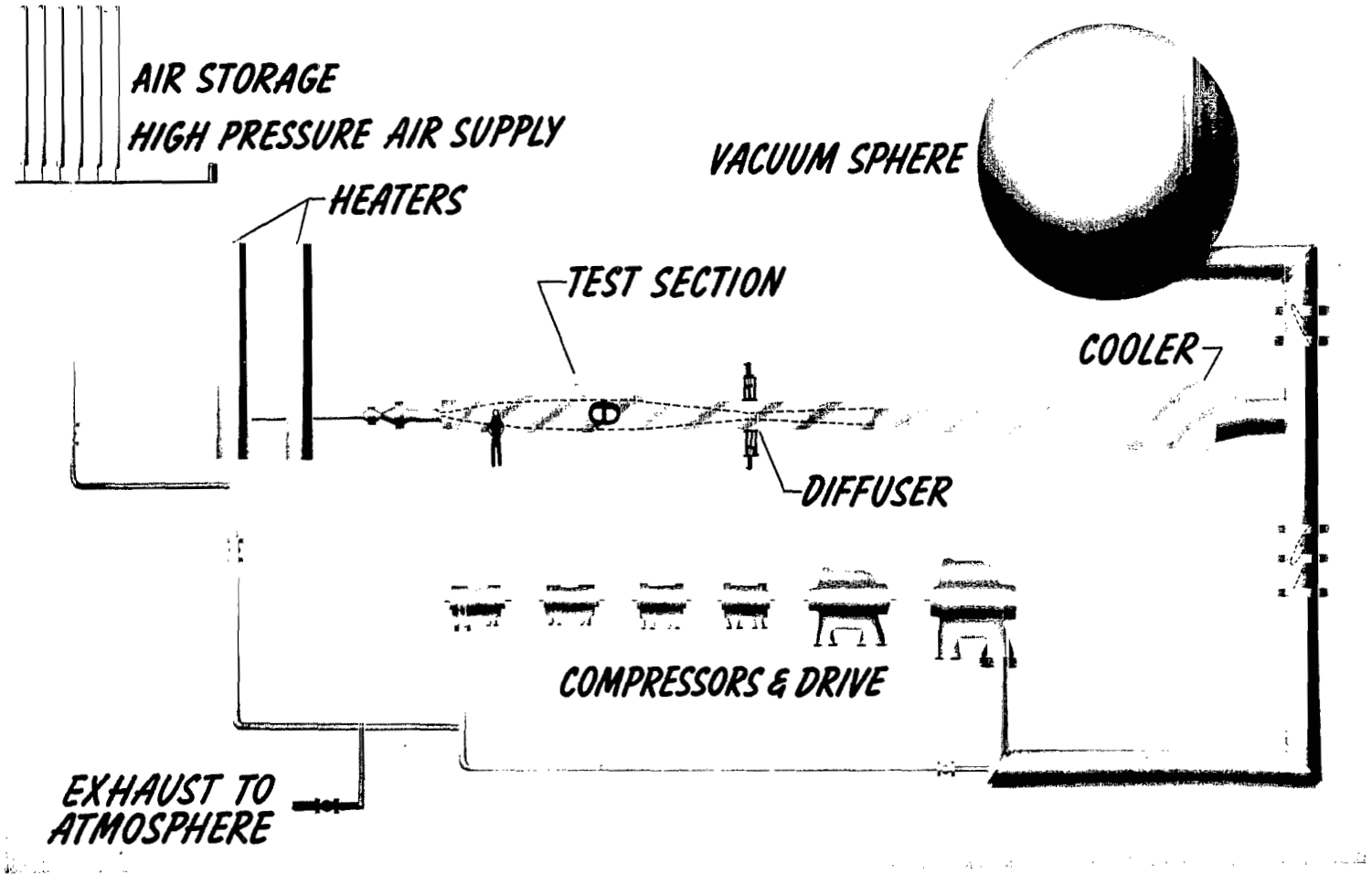

Figure 2.- Schematic diagram of the facility. L-1990.1

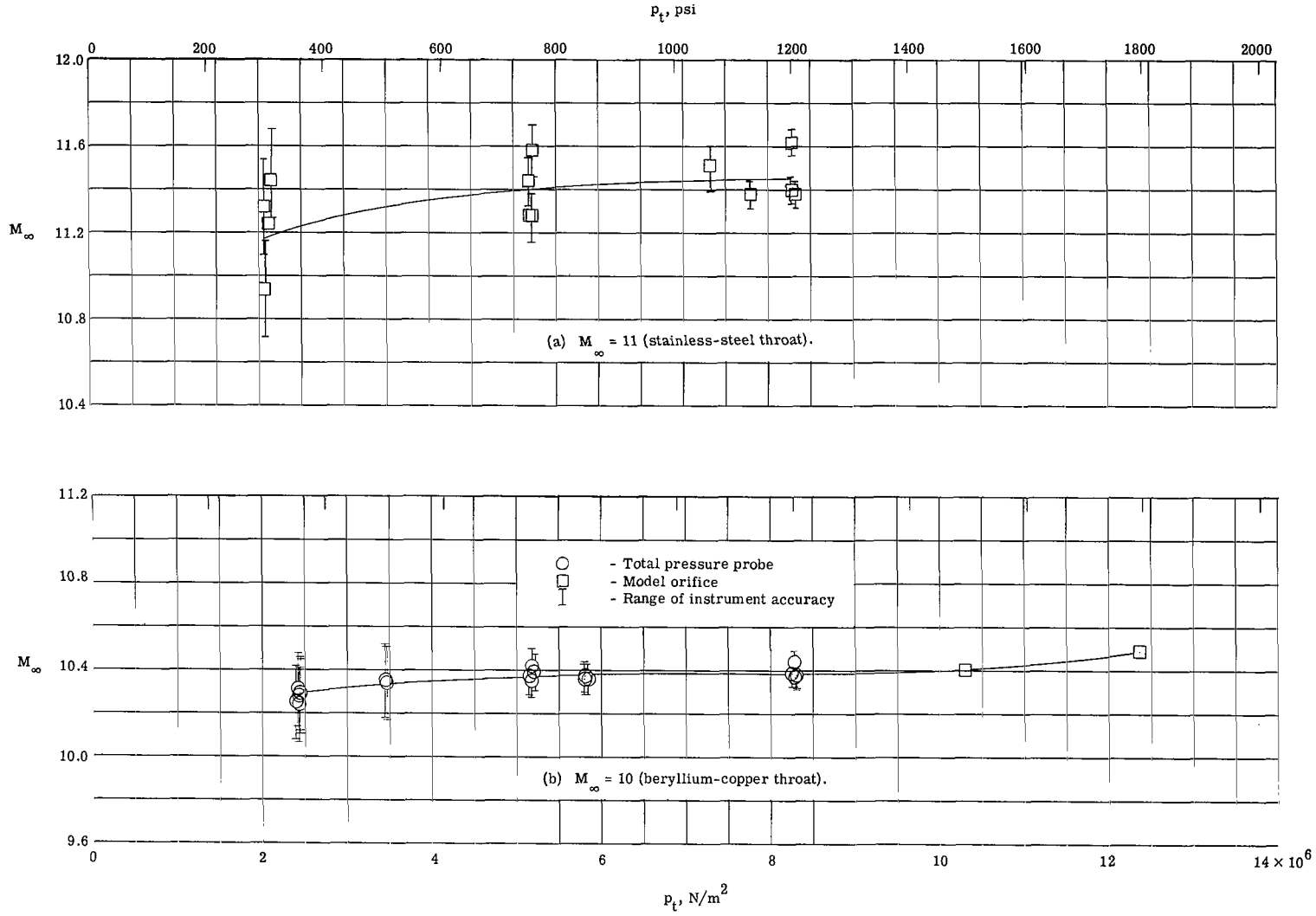

Figure 3.- Mach number calibration.

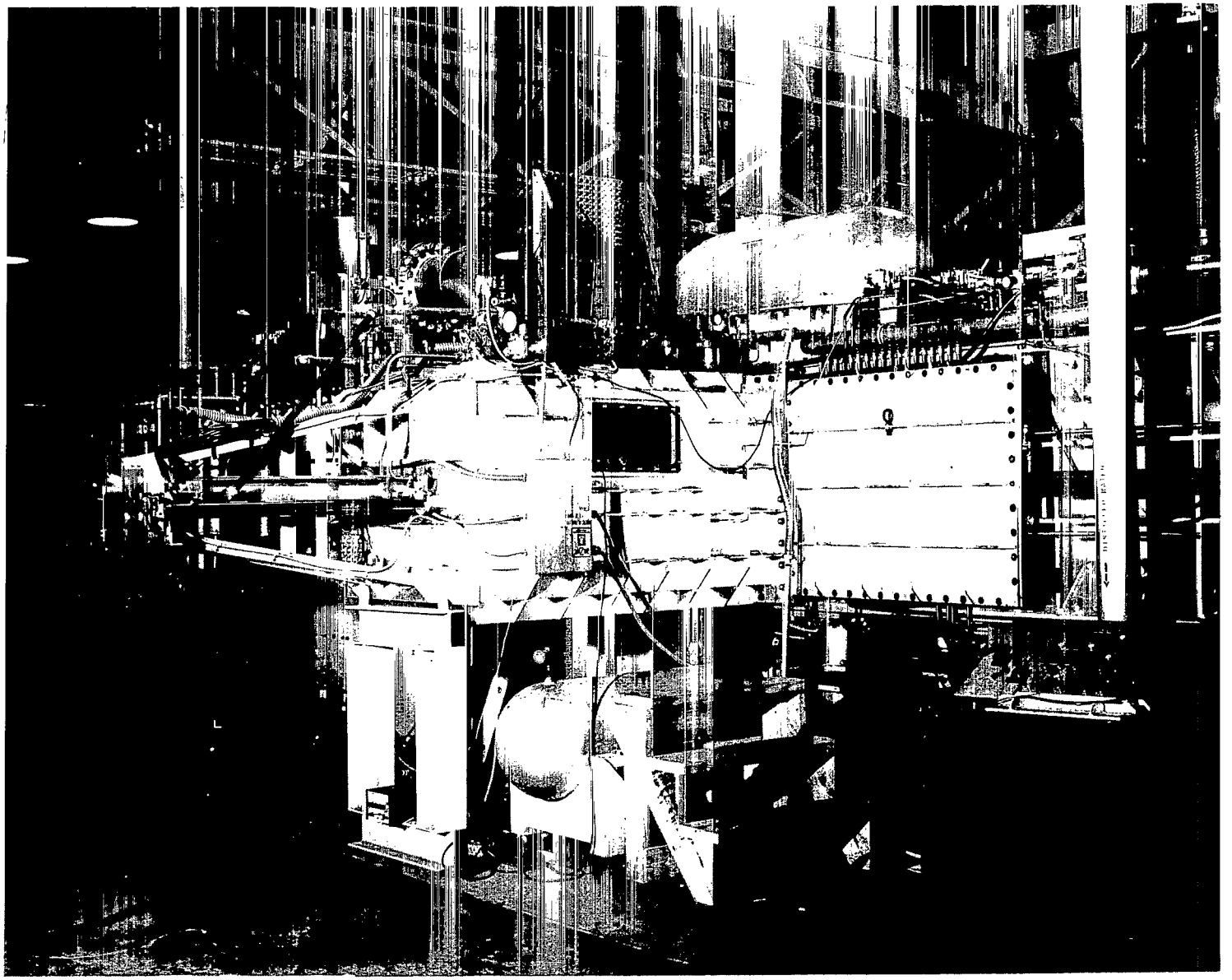

Figure 4.- Injection box.

L-65-5825

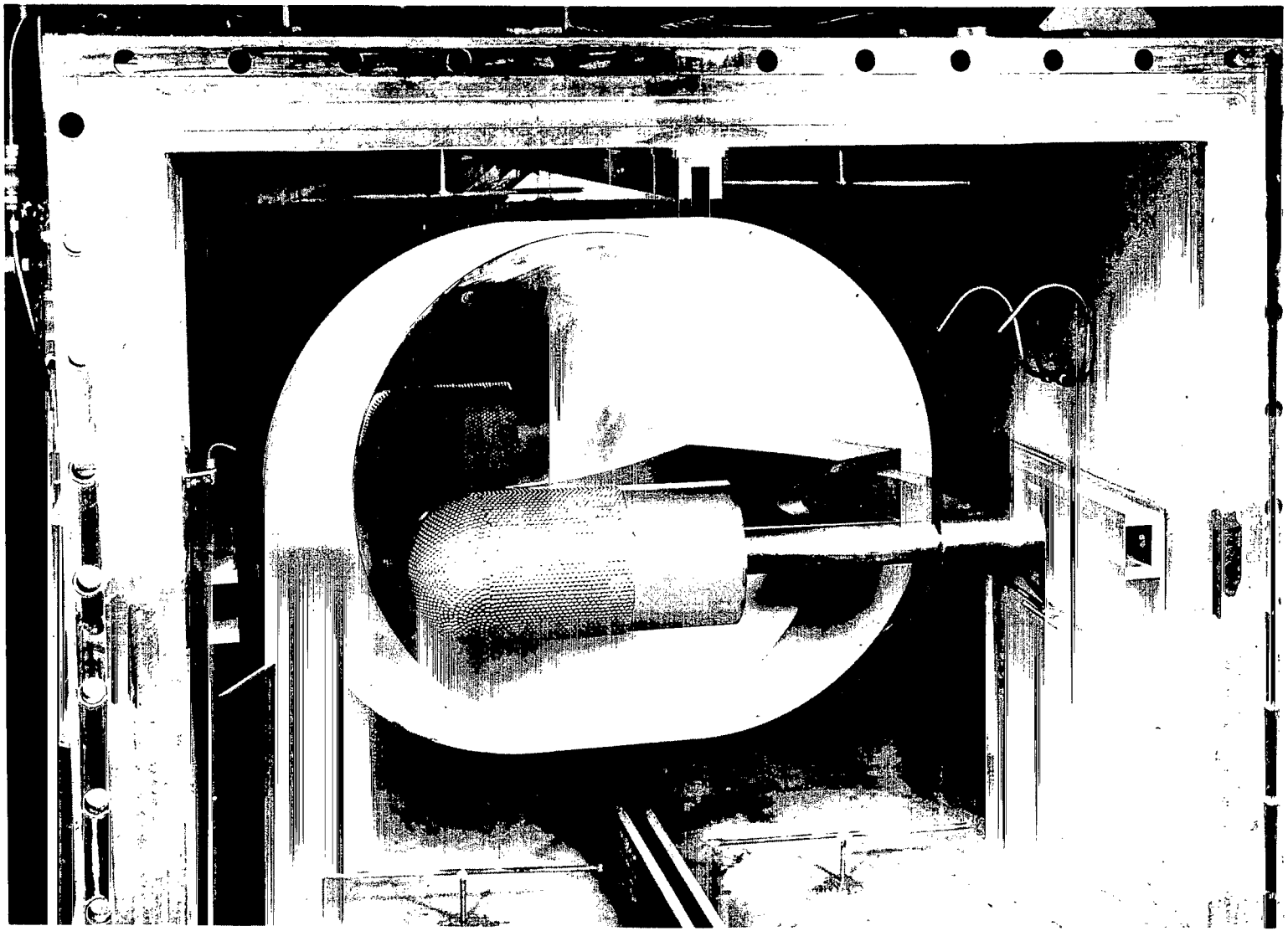

Figure 5.- Model IV mounted on injection strut.

L-66-2146

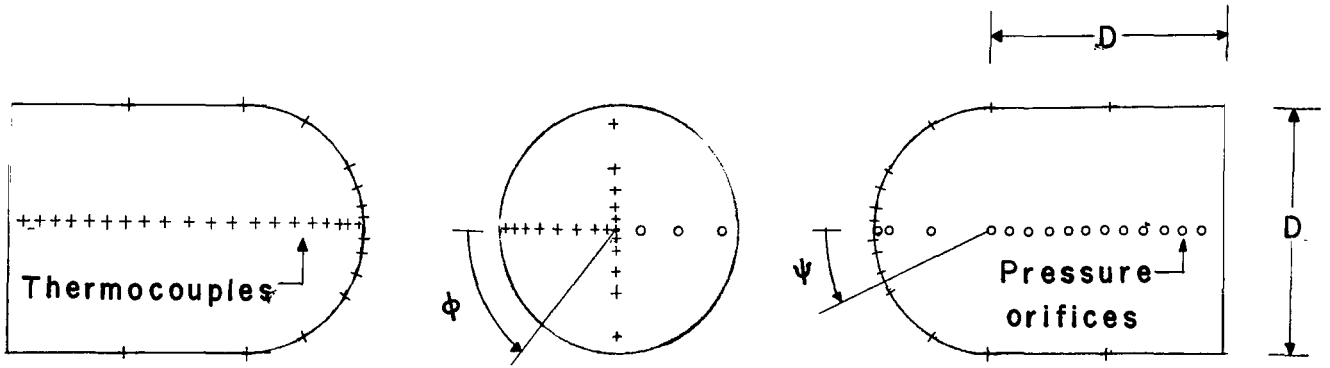

Model	Roughness		
	Height; k, mm. (in.)	Spacing	
		l, mm.(in.)	z, mm.(in.)
I	0	0	0
II	0.6(.025 in)	2.2(.087 in)	2.5(.1 in)
III	0.6(.025 in)	4.4(.17 in)	5.1(.2 in)
IV	1.3(.05 in)	4.4(.17 in)	5.1(.2 in)
V	.1(.004 in)	—	—

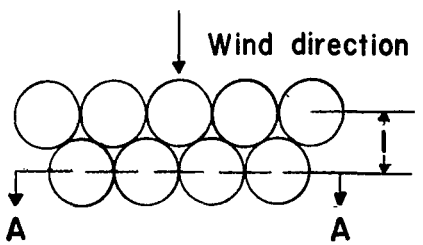

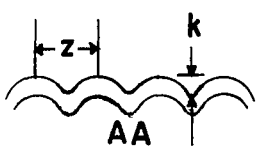

Note-Pressure orifices are located in valleys.

Figure 6.- Hemisphere-cylinder model. D = 15 cm (6 in.).

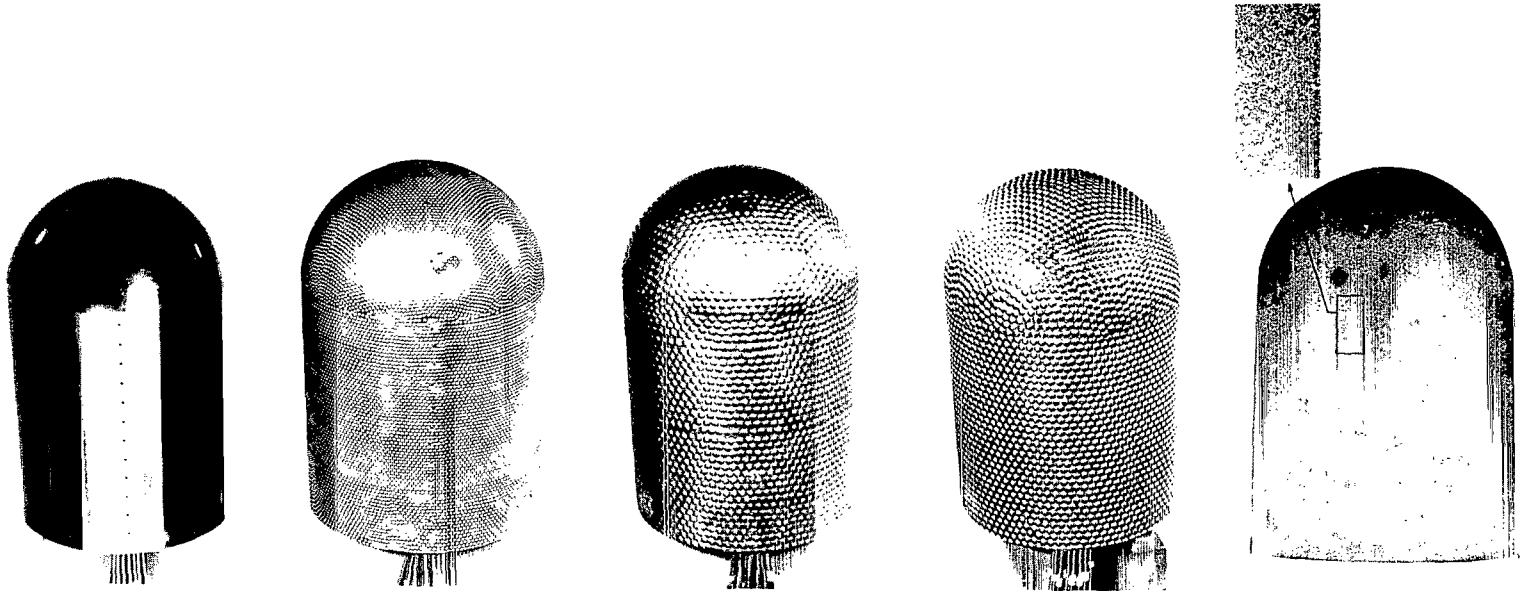

(a) Model I
smooth

(b) Model II
k=0.6mm.
z=2.5mm.
l=2.2mm.

(c) Model III
k=0.6mm.
z=5.1mm.
l=4.4mm.

(d) Model IV
k=1.3mm.
z=5.1mm.
l=4.4mm.

(e) Model V
k=0.1mm.
copper nodule

Figure 7.- Photographs of model surfaces.

L-66-7634

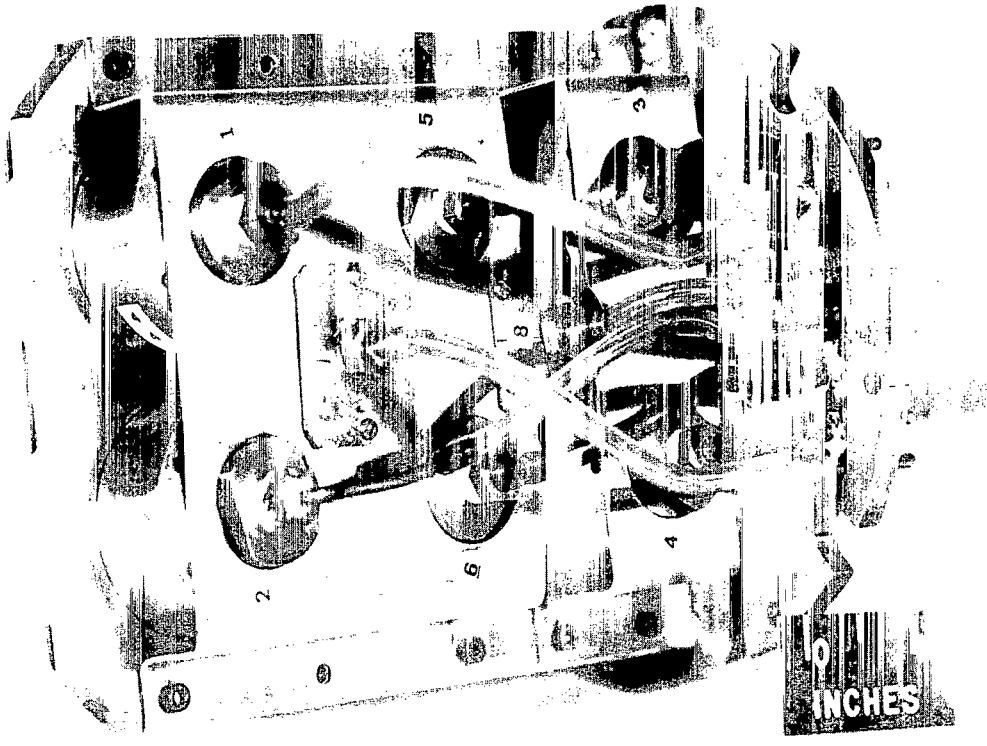

Figure 8.- Model surface support system, transducers, and instrumentation junctions. L-66-7635

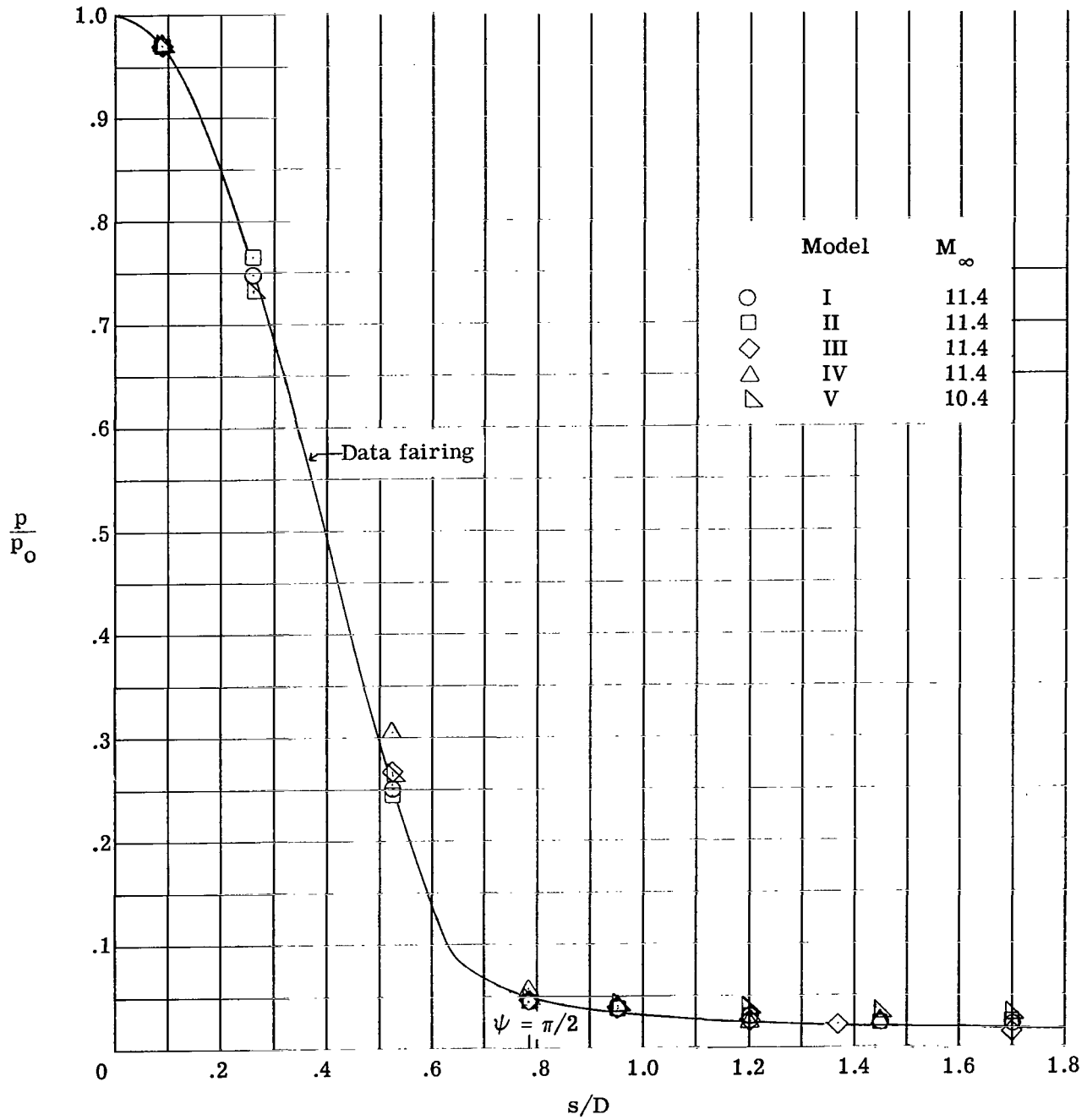

Figure 9.- Model pressure distributions at $p_t = 8.28 \times 10^6$ N/m^2 (1200 psia).

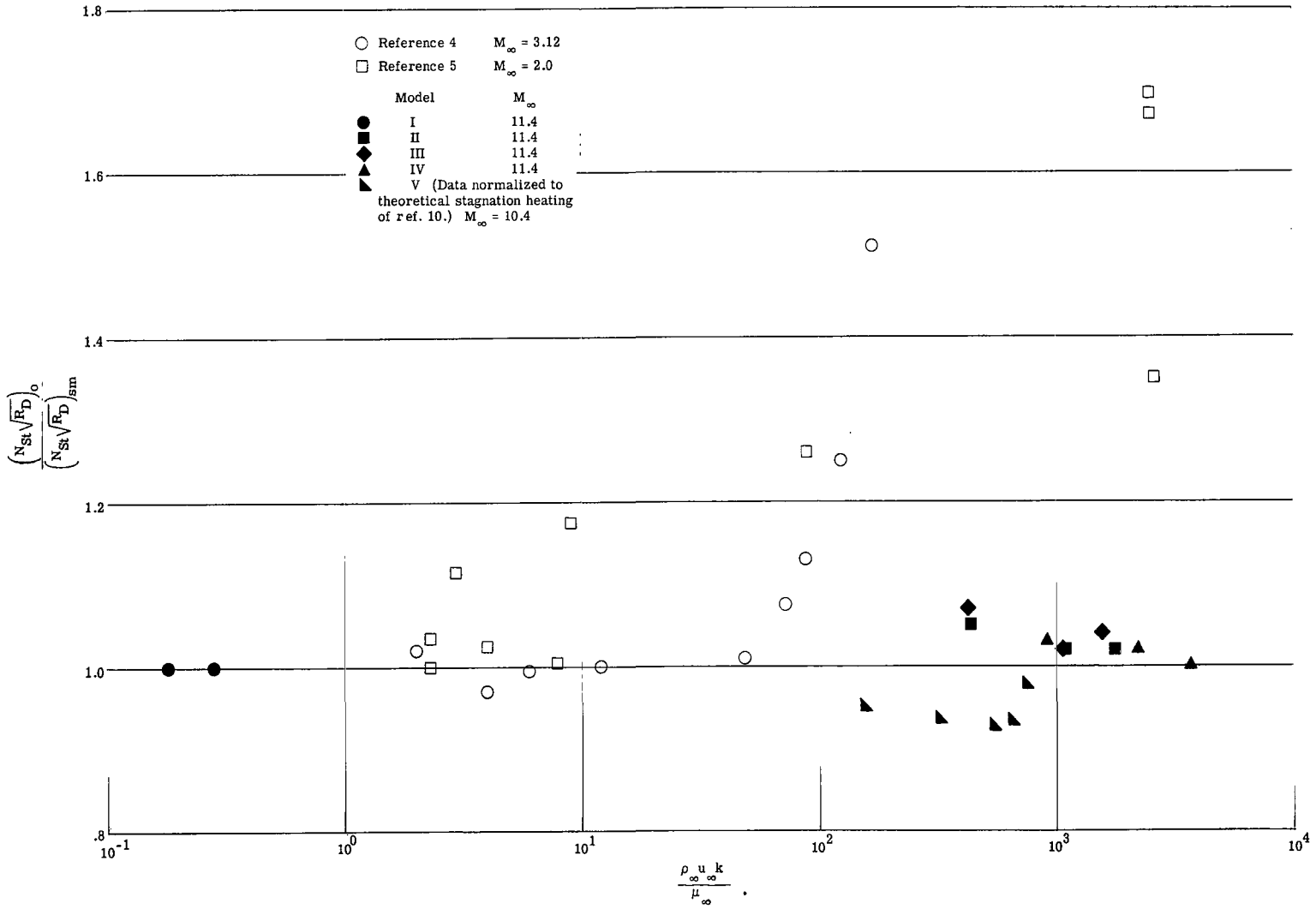

Figure 10.- Variation of stagnation-point heat transfer with free-stream roughness Reynolds number.

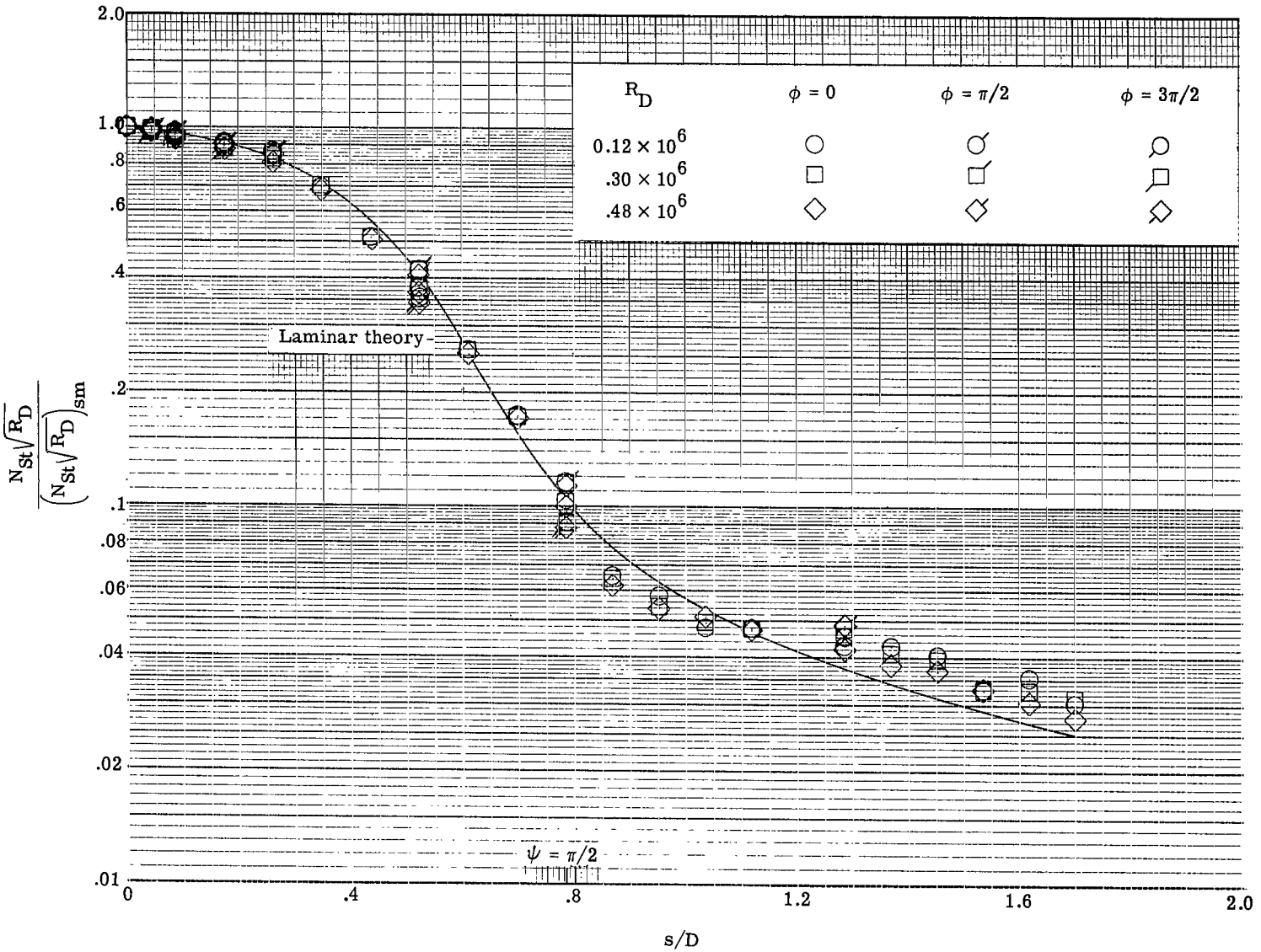

(a) Model I (smooth).

Figure 11.- Model heat-transfer distributions at $M_\infty = 11.4$.

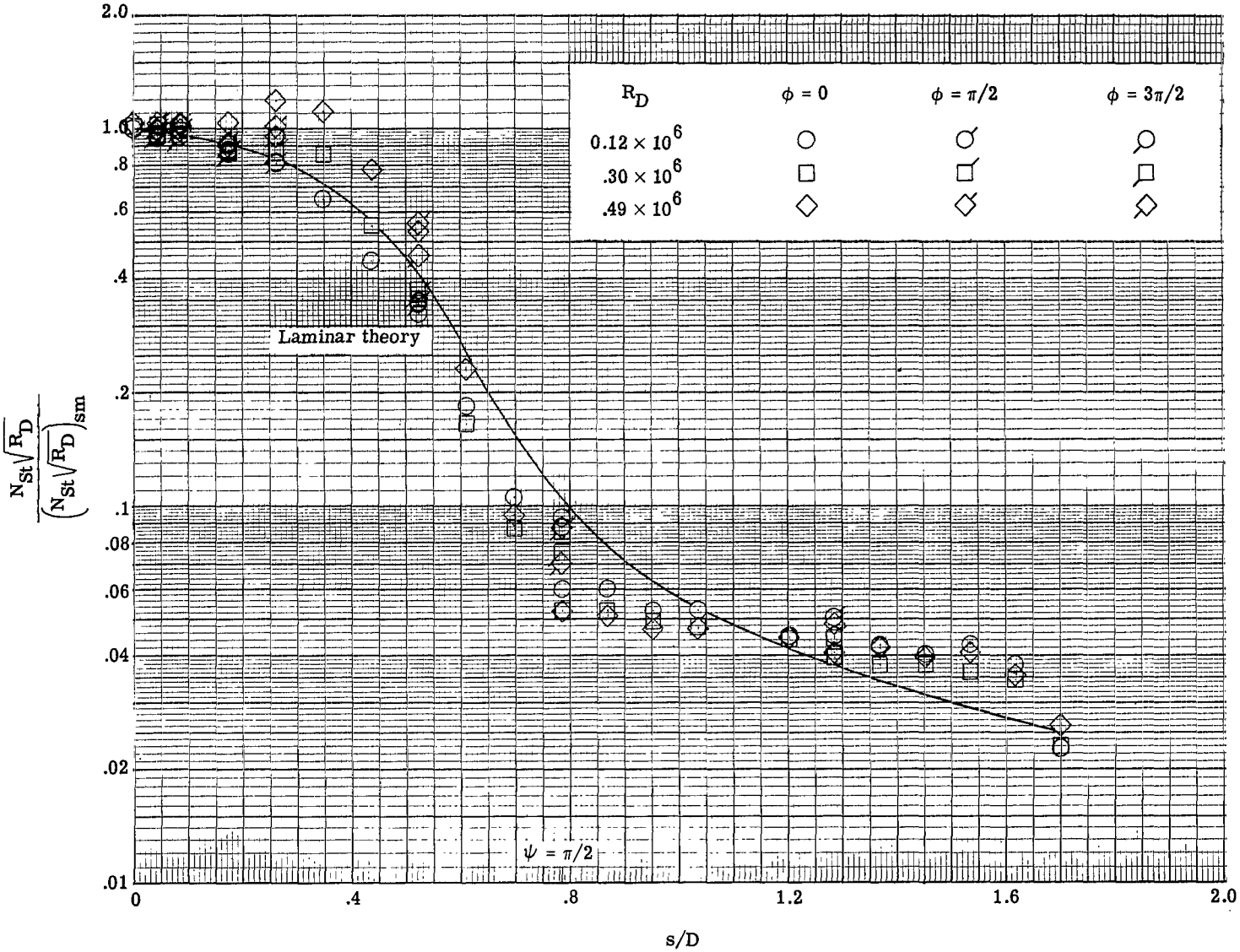

(b) Model II (k = 0.6 mm; z = 2.5 mm; and ℓ = 2.2 mm).

Figure 11.- Continued.

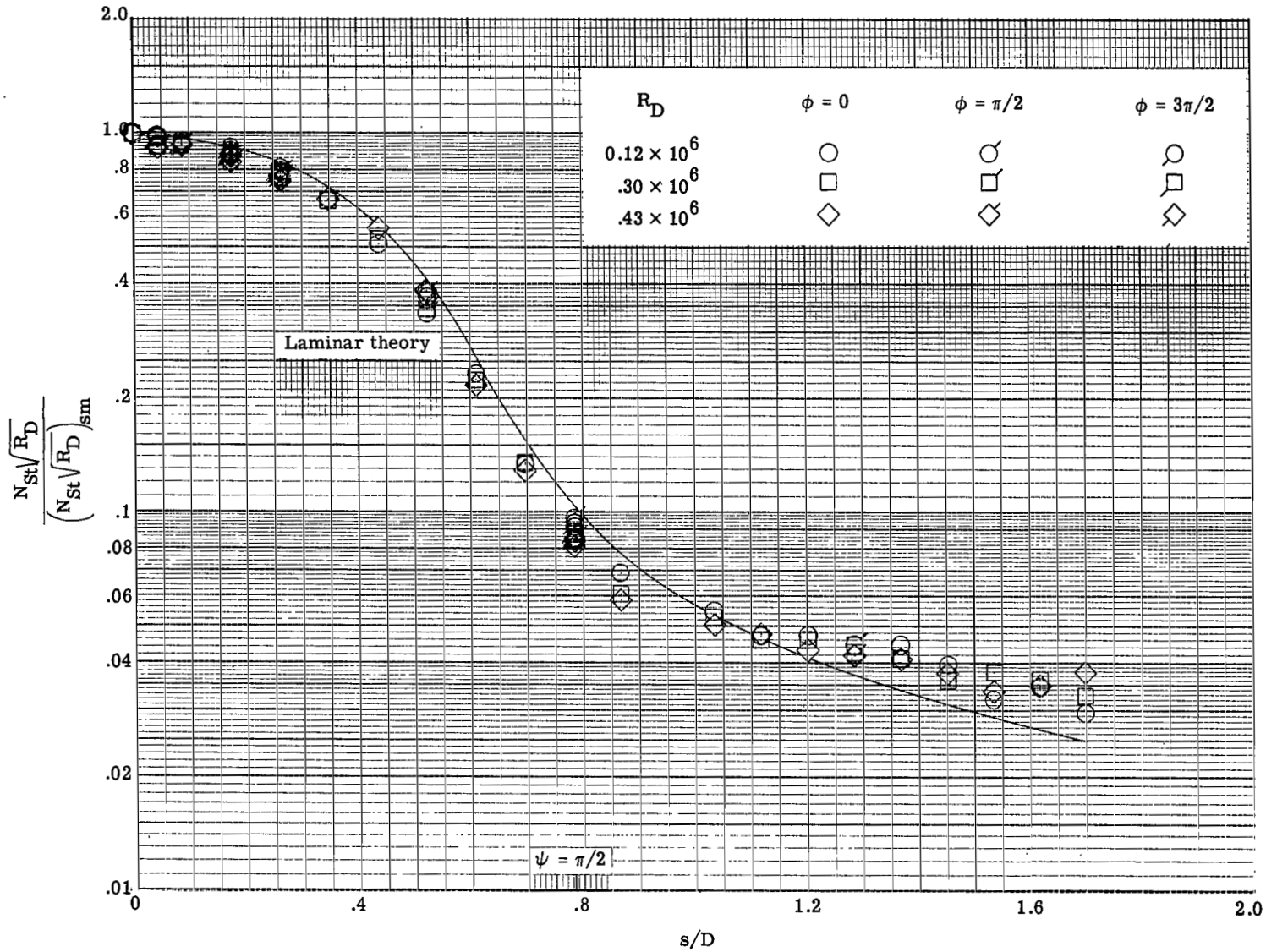

(c) Model III (k = 0.6 mm; z = 5.1 mm; and ℓ = 4.4 mm).

Figure 11.- Continued.

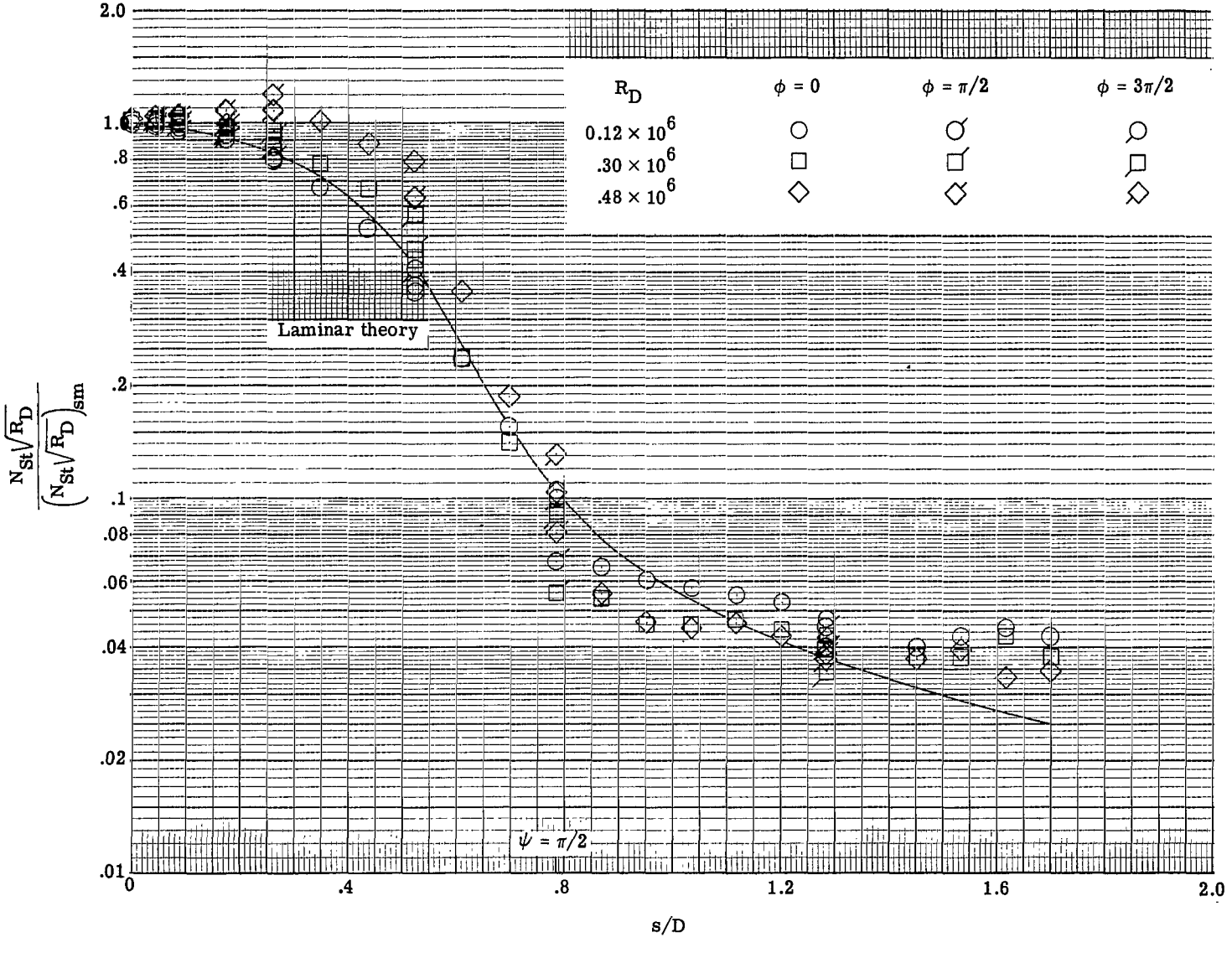

(d) Model IV (k = 1.3 mm; z = 5.1 mm; and ℓ = 4.4 mm).

Figure 11.- Concluded.

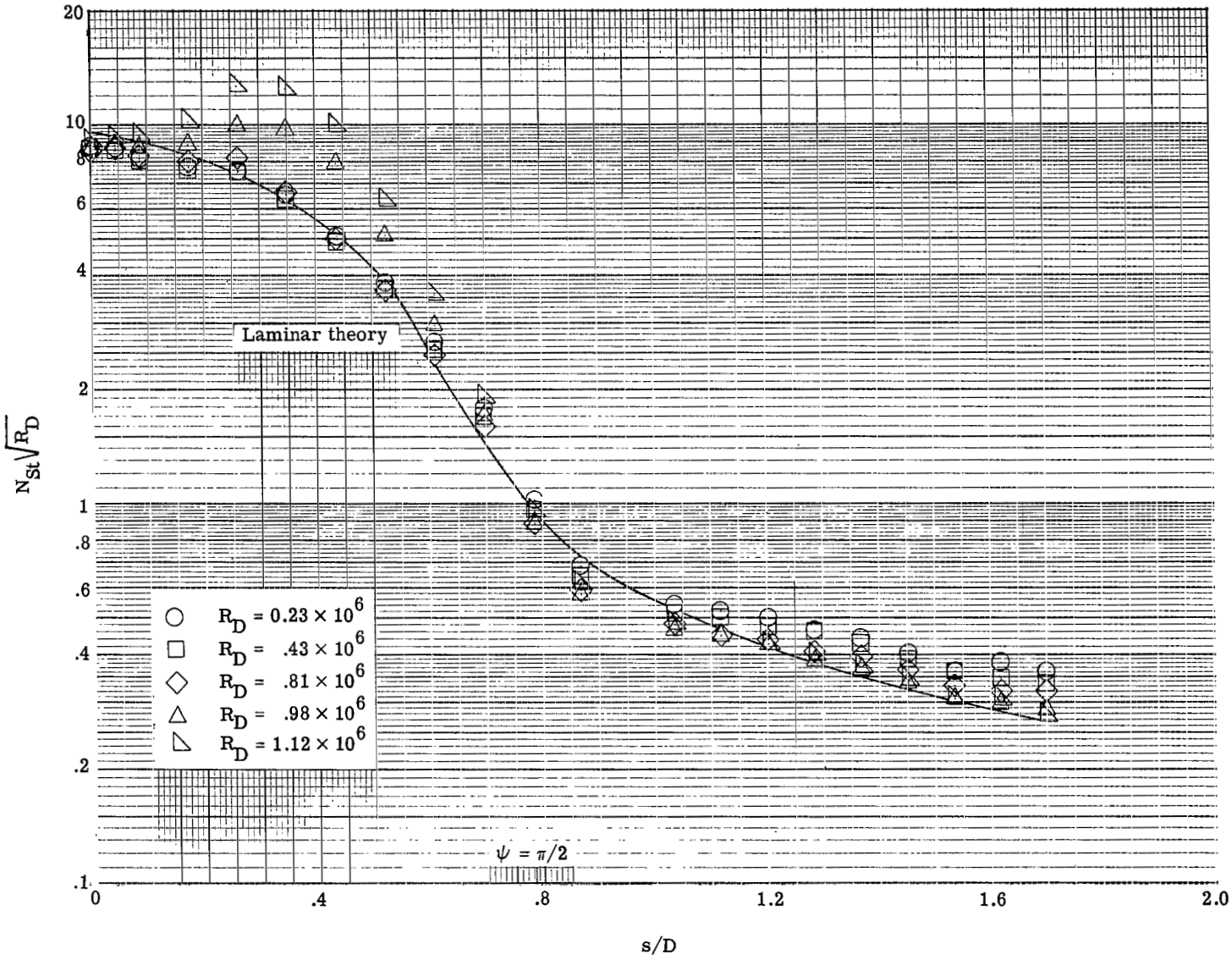

Figure 12.- Model V heat-transfer distribution at M_∞ = 10.4 in. and Φ = 0. (k = 0.1 mm.)

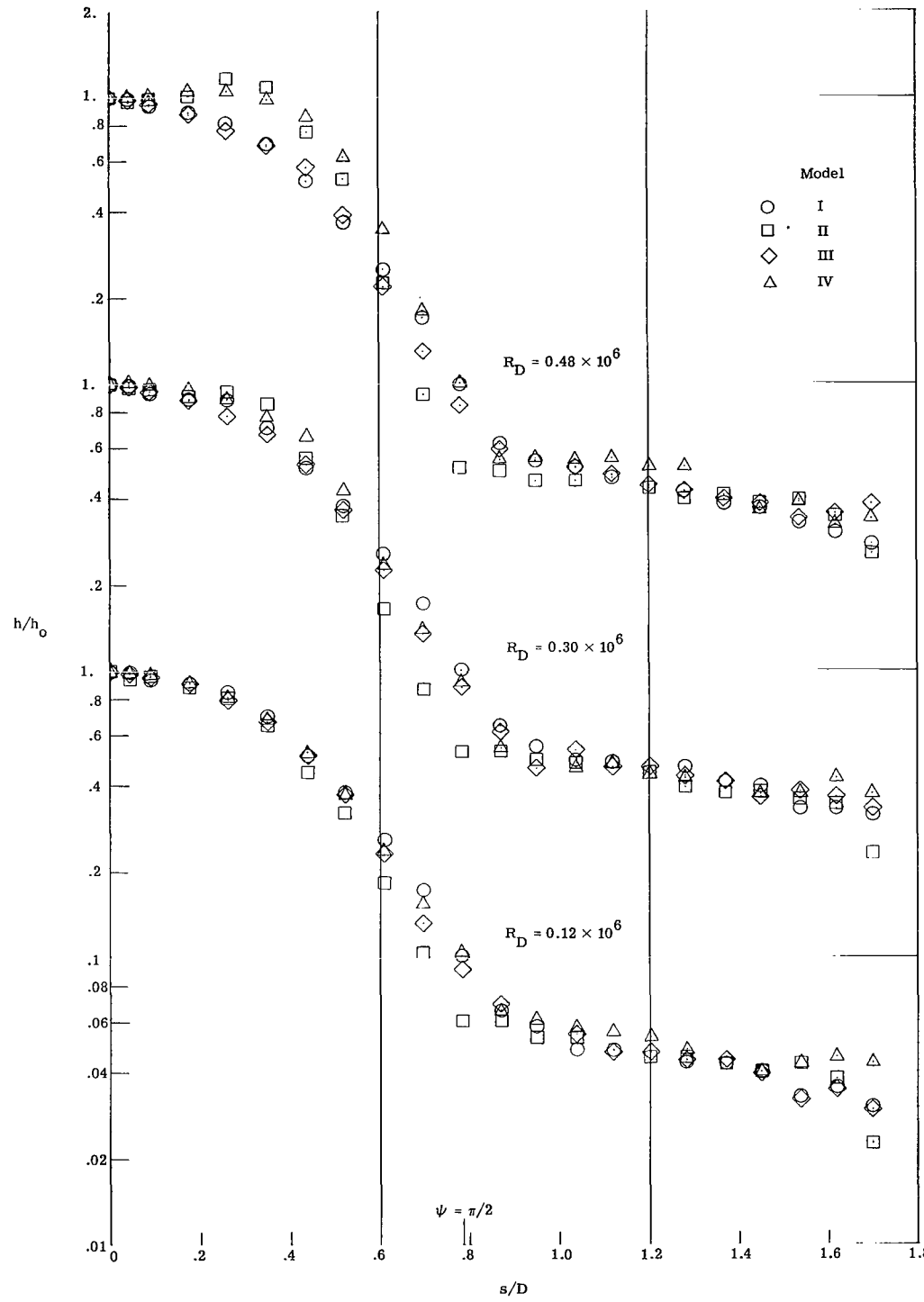

Figure 13.- Distribution of local to stagnation-point heat-transfer coefficients at various Reynolds numbers. ($M_\infty = 11.4$.)

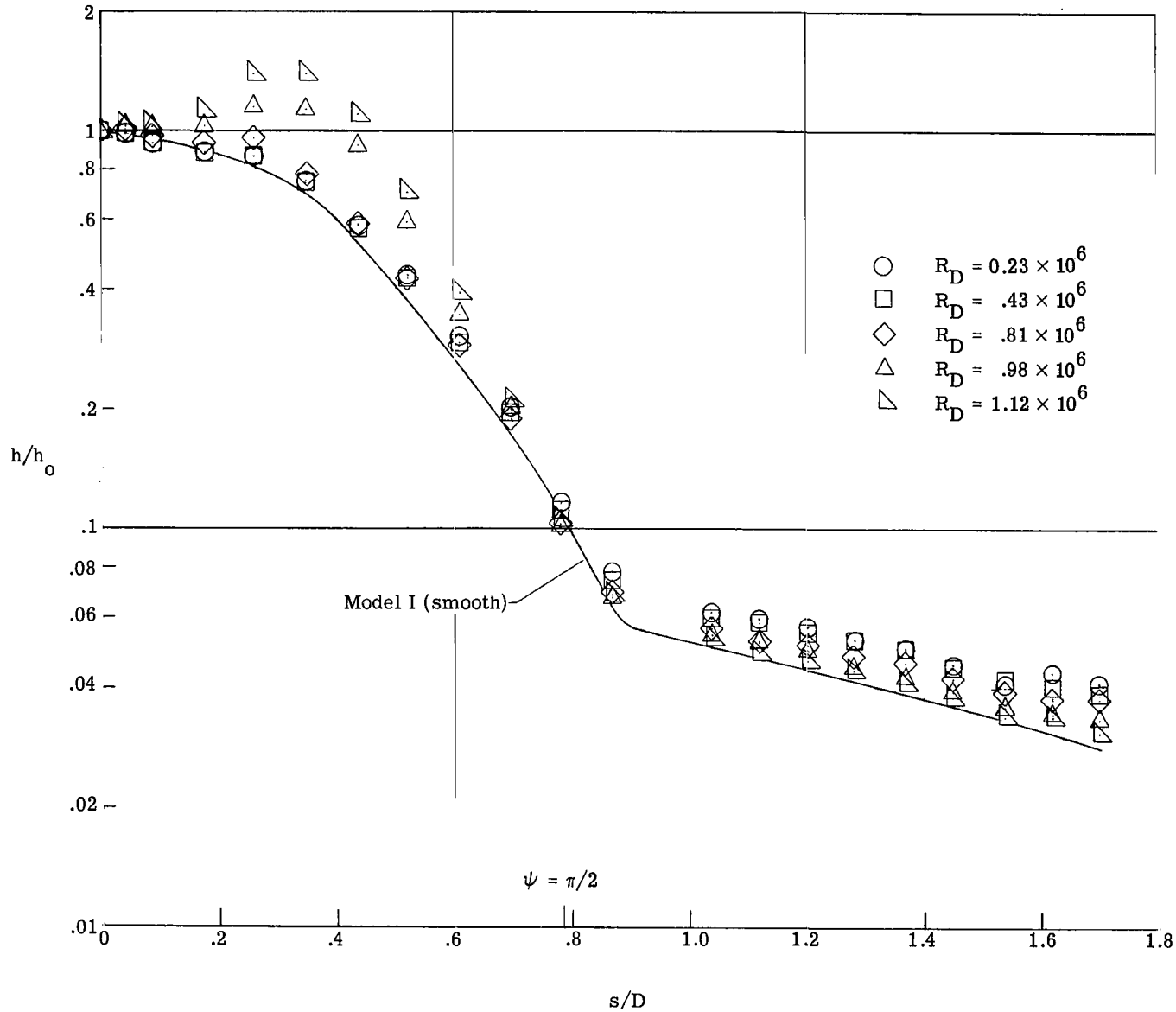

Figure 14.- Distribution of local to stagnation-point heat-transfer coefficients for model V at Mach 10.4 compared with fairing of model I (smooth) data at $R_D = 0.484 \times 10^6$ and Mach 11.4.

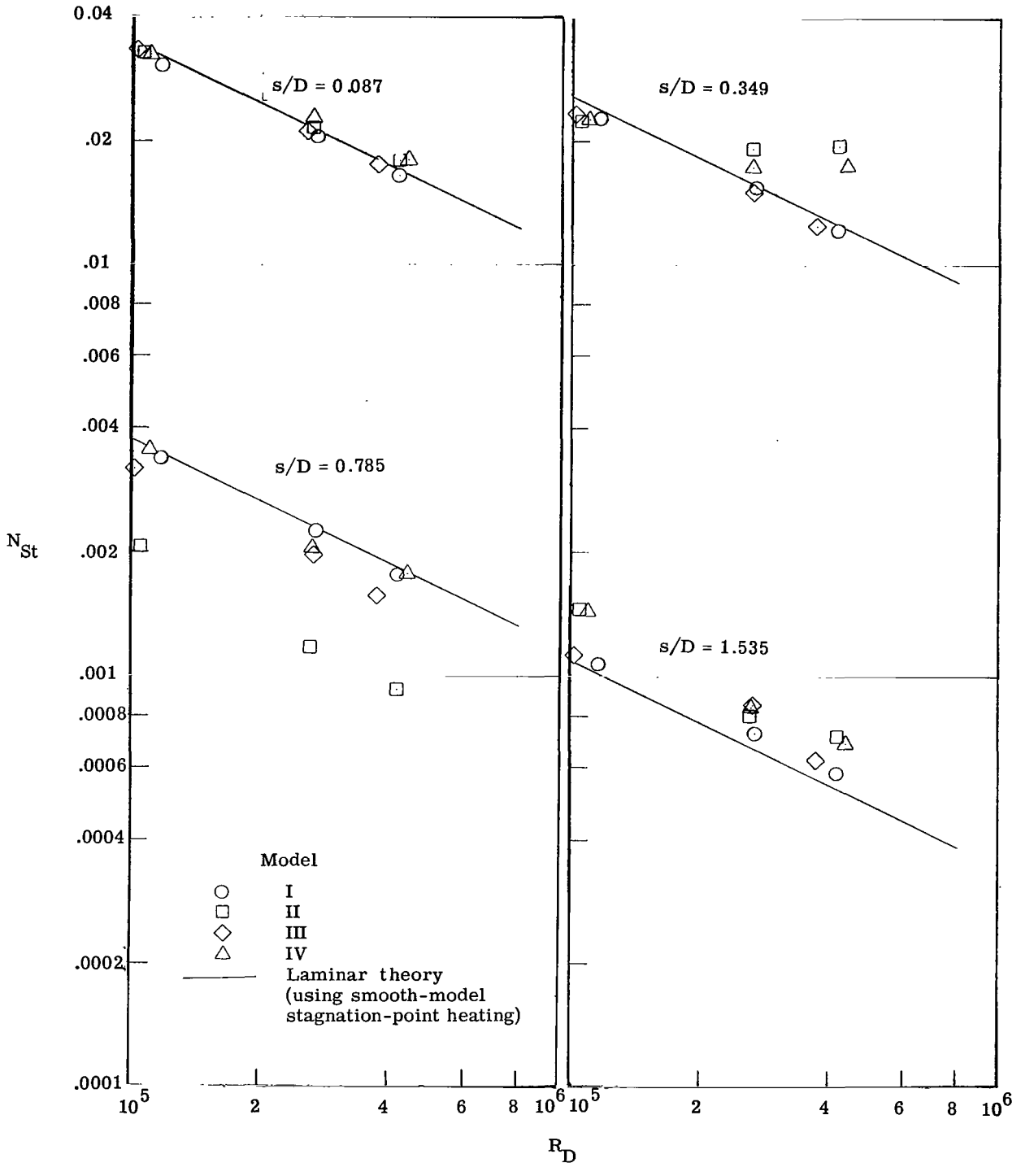

Figure 15.- Heat transfer at various model locations as a function of free-stream Reynolds number at $M_\infty = 11.4$.

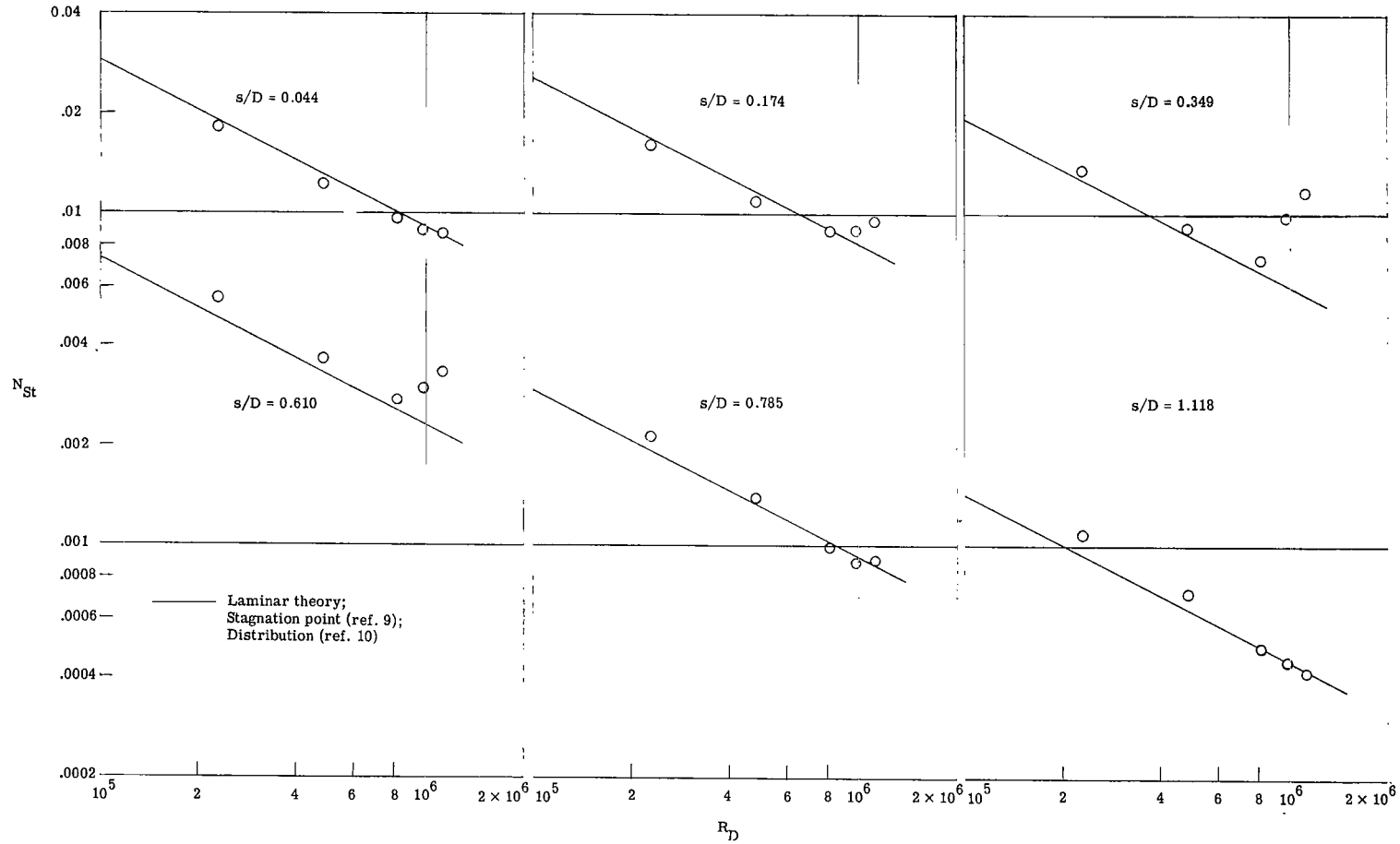

Figure 16.- Heat transfer at various locations on model V (copper nodule) as a function of free-stream Reynolds number at $M_\infty = 10.4$.

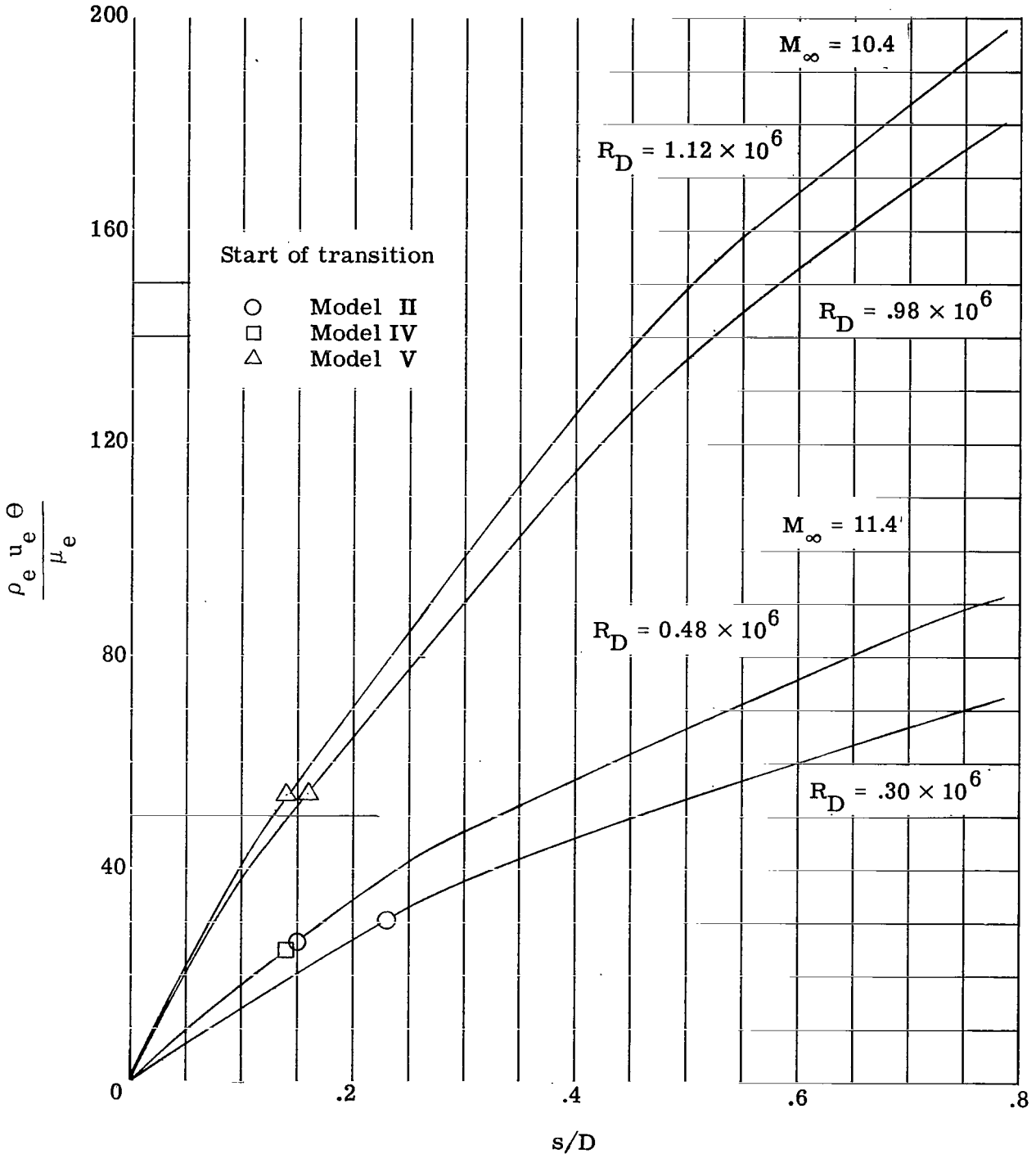

Figure 17.- Momentum thickness Reynolds number distribution on the hemisphere.

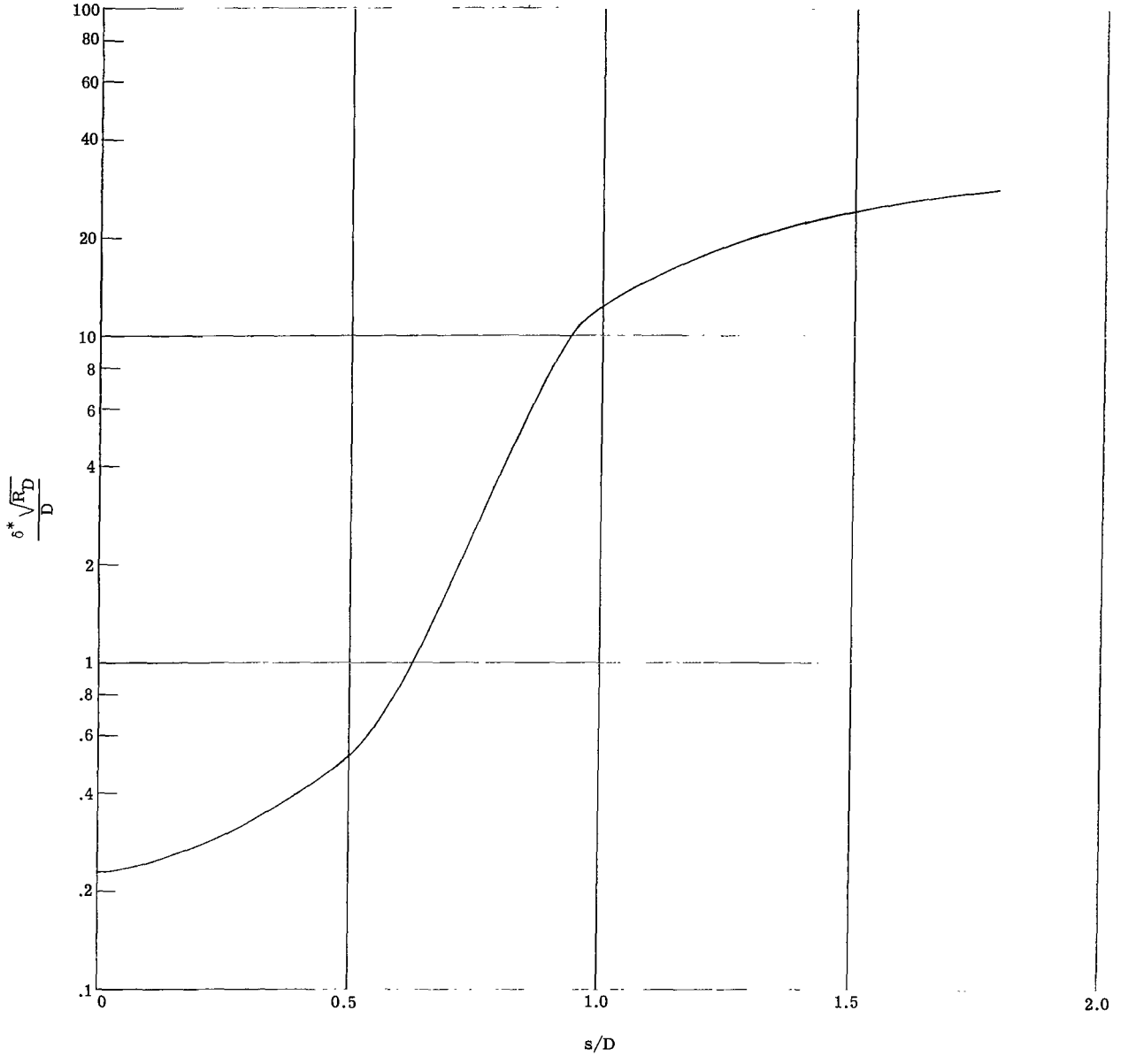

Figure 18.- Laminar boundary-layer displacement thickness on hemisphere-cylinder at $M_\infty = 10.4$.

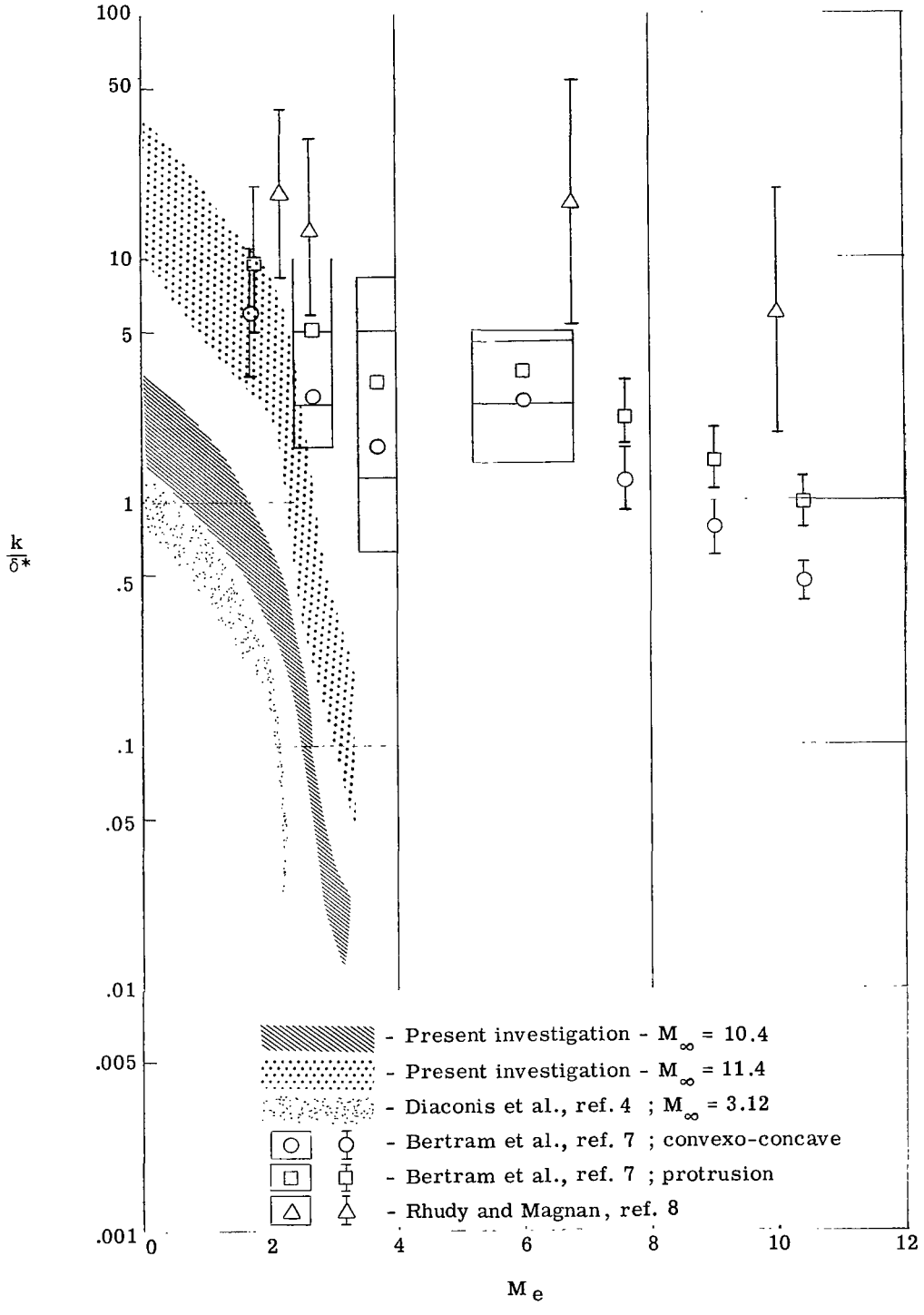

Figure 19.- Ratio of roughness height to laminar boundary-layer displacement thickness.

"The aeronautical and space activities of the United States shall be conducted so as to contribute . . . to the expansion of human knowledge of phenomena in the atmosphere and space. The Administration shall provide for the widest practicable and appropriate dissemination of information concerning its activities and the results thereof."

—NATIONAL AERONAUTICS AND SPACE ACT OF 1958

NASA SCIENTIFIC AND TECHNICAL PUBLICATIONS

TECHNICAL REPORTS: Scientific and technical information considered important, complete, and a lasting contribution to existing knowledge.

TECHNICAL NOTES: Information less broad in scope but nevertheless of importance as a contribution to existing knowledge.

TECHNICAL MEMORANDUMS: Information receiving limited distribution because of preliminary data, security classification, or other reasons.

CONTRACTOR REPORTS: Technical information generated in connection with a NASA contract or grant and released under NASA auspices.

TECHNICAL TRANSLATIONS: Information published in a foreign language considered to merit NASA distribution in English.

TECHNICAL REPRINTS: Information derived from NASA activities and initially published in the form of journal articles.

SPECIAL PUBLICATIONS: Information derived from or of value to NASA activities but not necessarily reporting the results of individual NASA-programmed scientific efforts. Publications include conference proceedings, monographs, data compilations, handbooks, sourcebooks, and special bibliographies.

Details on the availability of these publications may be obtained from:

SCIENTIFIC AND TECHNICAL INFORMATION DIVISION

NATIONAL AERONAUTICS AND SPACE ADMINISTRATION

Washington, D.C. 20546